

# Study on the global minimum and $H \rightarrow \gamma\gamma$ in the Dirac scotogenic model

Raghavendra Srikanth Hundi\*

*Department of Physics, Indian Institute of Technology Hyderabad, Kandi - 502 284, India*



(Received 10 March 2023; accepted 18 June 2023; published 6 July 2023)

We have analyzed the vacuum structure of the Dirac scotogenic model, whose scalar sector consists of two complex Higgs doublets and a real singlet field. In this model, the standard model like the Higgs doublet acquires the nonzero vacuum expectation value (VEV), whereas, the other two fields acquire zero VEVs. This pattern of VEVs constitutes a minimum, which is the desired vacuum of the model. After analyzing the scalar potential of this model, we have found that other vacua are also possible in this model. We have shown that plenty of parameter space exists where the desired vacuum of this model is the global minimum. We have studied the implications of the scalar sector of this model on the observable quantity of signal strength of Higgs to diphoton decay. After evaluating this quantity, we have found that the current experimental values of this quantity can be fitted in this model. Lastly, we have studied on the possibility of making any of the additional scalar fields of this model as a candidate for dark matter.

DOI: [10.1103/PhysRevD.108.015006](https://doi.org/10.1103/PhysRevD.108.015006)

## I. INTRODUCTION

With the discovery of Higgs boson at the LHC [1,2], the spontaneous breaking of electroweak symmetry has been verified. In the standard model (SM), the breaking of this symmetry is explained by postulating a single scalar Higgs doublet [3–7], which acquires the nonzero vacuum expectation value (VEV) at the minimum of the scalar potential. A consequence of this breaking mechanism is the existence of the Higgs boson, which is found in the LHC. As of now, the properties of the Higgs boson, which are measured at the LHC, agrees with the SM predictions [8]. However, more work is to be done in order to precisely measure the couplings of Higgs boson to all the SM particles. On the other hand, several reasons exist for the extension of the SM [9,10]. As a result of this, it is worth exploring theories by proposing additional Higgs doublets. A minimal extension to the SM, in this aspect, is the two Higgs doublet model (2HDM) [11], where the field content is the same as that of the SM apart from an extra scalar Higgs doublet.

In the SM, at the minimum of the scalar potential, the VEV of the scalar doublet breaks only the electroweak symmetry. In contrast to this, in the 2HDM, both the Higgs doublets can acquire VEVs in such a way that, in addition to the electroweak symmetry,  $CP$  and charge symmetries can also be broken spontaneously [12,13]. Different forms

of VEVs to the Higgs doublets are possible in the 2HDM, due to the parameter choice of the model. As a result of this, in the 2HDM, the possible vacua are categorized as follows [12,13]: (i) neutral minimum, (ii)  $CP$ -violating minimum, and (iii) charge-breaking minimum. Here, neutral minimum breaks only the electroweak symmetry. Whereas,  $CP$ - and charge-breaking minima break the respective symmetries, in addition to the electroweak symmetry.  $CP$ -violating minimum is phenomenologically acceptable, however, charge-breaking minimum should be avoided since violation of charge symmetry is not found in experiments. Theoretically it is demonstrated that, in the 2HDM, a neutral minimum do not coexist with either  $CP$ - or charge-breaking minima [12–15]. In other words, it is possible to choose a parameter region of the scalar potential of the 2HDM in such a way that the minimum breaks only the electroweak symmetry spontaneously, and moreover, this can be the global minimum. This result is appealing, and it makes the 2HDM as a viable candidate for the extension of the SM.

The result mentioned above is valid in any model where the scalar sector contains only two Higgs doublets. Several models are proposed with only the two Higgs doublets, in order to explain the limitations of the SM [9,10]. One among these is the scotogenic model [16], whose motivation is to explain the smallness of neutrino masses and the existence of dark matter. This model contains an additional and exact discrete symmetry  $Z_2$ , whose purpose is to generate neutrino masses at 1-loop level and also to accommodate a candidate for dark matter. In order to achieve the motivation of this model, one of the two Higgs doublets of this model should acquire nonzero VEV and the other one should acquire zero VEV. We can consider this pattern of VEVs to the Higgs

\*rshundi@phy.iith.ac.in

*Published by the American Physical Society under the terms of the Creative Commons Attribution 4.0 International license. Further distribution of this work must maintain attribution to the author(s) and the published article's title, journal citation, and DOI. Funded by SCOAP<sup>3</sup>.*

doublets as the desired vacuum of the scotogenic model. However, by minimizing the scalar potential of this model, it is possible for both the Higgs doublets to acquire different patterns of VEVs, and thus generate different possible vacua. Topics on this subject are discussed in [17,18], and it is shown that it is possible to make the desired vacuum of the scotogenic model as the global minimum by restricting the parameter space of the model. See Refs. [19,20] for alternative proposals on scotogenic mechanism in composite Higgs models.

In the scotogenic model [16], neutrinos are Majorana particles. Since there is no indication from experiments on the Majorana nature of neutrinos, *a priori*, it is worth it to construct models based on the Dirac nature of neutrinos. It is for this reason the scotogenic model has been modified into the Dirac scotogenic model [21], where the neutrinos are purely Dirac particles. In this later model, three copies of Weyl singlet fermions  $\nu_\alpha^c$ ,  $N_k$ ,  $N_k^c$  are introduced. Here,  $\alpha = e, \mu, \tau$ , which is the generation index of the lepton family and  $k = 1, 2, 3$ .  $N_k$  and  $N_k^c$  combine to give massive Dirac fermions  $N_k^D$ . Whereas,  $\nu_\alpha^c$  combine with left-handed neutrinos of the lepton doublets to form Dirac neutrinos  $\nu_\alpha^D$ . To forbid Majorana masses for the above Weyl fermions and to conserve the lepton number, an additional and exact symmetry  $U(1)_{B-L}$  is proposed. In the scalar sector of this model, there exist two complex Higgs doublets ( $\Phi, \eta$ ) and a real scalar singlet ( $\chi$ ). Here,  $\Phi$  is the SM-like Higgs doublet. This model has an additional symmetry  $Z_2^{(A)} \times Z_2^{(B)}$ , which prevents masses to Dirac neutrinos at tree level and generates them at 1-loop level [21]. The construction of the model is such that the  $Z_2^{(A)}$  symmetry is softly broken but  $Z_2^{(B)}$  is exact symmetry. Hence, the lightest charged particle under  $Z_2^{(B)}$  can be a viable candidate for dark matter.

Like in the case of the scotogenic model, in the Dirac scotogenic model as well, the scalar fields should acquire VEVs in a specific pattern in order to generate masses for neutrinos at 1-loop level in a consistent way. This pattern is such that only  $\Phi$  acquires nonzero VEV, whereas,  $\eta$  and  $\chi$  acquire zero VEVs [21]. We expect this pattern of VEVs to constitute a minimum of the model in some parameter region of it. On the other hand, with the description we have given for the cases of the 2HDM and scotogenic model, one can expect other possible minima for the Dirac scotogenic model, apart from the desired minimum which is mentioned above. A noteworthy point is that the scalar content of the Dirac scotogenic model is different from that of the 2HDM. Hence, the results we described above for the case of the 2HDM need not be applicable to the Dirac scotogenic model. More specifically, we may expect some charge-breaking minima to coexist with the desired minimum of this model. As a result of this, we need to know if the desired minimum of this model can be made as the global minimum.

In this work, after analyzing the scalar potential, we describe all possible inequivalent vacua of the Dirac scotogenic model. We have found that, including the desired minimum of this model, there can exist 11 different vacua, which includes three charge-breaking minima. As part of our investigation on global minimum, we have studied if the desired minimum of this model can coexist with other possible vacua of the model. In our numerical analysis, we have found that the desired minimum of this model does not coexist with charge-breaking minima in the viable parameter space of this model. We have justified this result by giving an analytical proof to it. On the other hand, the desired minimum of this model is found to coexist with certain other minima of the model. In the case that the desired minimum of this model coexists with other minima, we have given the conditions that need to be satisfied in order to make the desired minimum of this model as the global minimum. We have shown that there exists plenty of parameter space where the desired minimum of this model is the global minimum.

The study on global minimum of the Dirac scotogenic model will have implications on the scalar sector of this model since the analysis is mainly concerned with the parameters of the scalar potential. One of the phenomenological implications of the scalar sector of this model is on the signal strength of the Higgs to diphoton decay  $H \rightarrow \gamma\gamma$ . The signal strength of  $H \rightarrow \gamma\gamma$ ,  $R_{\gamma\gamma}$  is measured in the LHC experiment, and its value is around 1 [8]. The additional contribution to the decay  $H \rightarrow \gamma\gamma$  in the Dirac scotogenic model [21] is due to the trilinear coupling of the Higgs with the charged component of  $\eta$  field. As a result of this, the contribution to  $R_{\gamma\gamma}$  is determined by the above trilinear coupling and also by the masses of components of  $\eta$  field. Since the couplings and masses of scalar fields are affected by the above described analysis of global minimum, we have studied its implications on  $R_{\gamma\gamma}$ . In our analysis, we have found that the experimental value of  $R_{\gamma\gamma}$  can be fitted in this model, irrespective of the fact that the desired minimum of this model coexists with other minima or not. The fitted value to  $R_{\gamma\gamma}$  in this model is found to be either less or greater than 1, depending on the parameter choice.

Another implication of the scalar sector of the Dirac scotogenic model is on the dark matter phenomenology [8]. As described above, in this model,  $Z_2^{(B)}$  is an exact symmetry. Hence, the lightest particle charged under the  $Z_2^{(B)}$  can be a candidate for dark matter. We have studied on the possibility of making any of the additional scalar fields of this model as a candidate for thermal cold dark matter.

The paper is organized as follows. In the next section, we give a brief description on the Dirac scotogenic model. In Sec. III, we describe all different possible minima of this model. In Secs. IV and V, we discuss making the desired minimum of this model as the global minimum. In Sec. VI, we present our study on the signal strength of Higgs to diphoton decay. In Sec. VII, we discuss the possibility of a

scalar dark matter candidate in this model. In Sec. VIII, we have compared the phenomenology of the Dirac scotogenic model with that of the scotogenic model. We present the conclusions of our work in Sec. IX. In the Appendix, we describe analytical arguments in order to justify some of the numerical results of Sec. V.

## II. DIRAC SCOTOGENIC MODEL

We have given a brief introduction to the Dirac scotogenic model [21] in Sec. I. In this work, we follow the original model of this, which is proposed in [21]. Apart from this, other models are also proposed which have the idea of scotogenic masses to Dirac neutrinos [22–28]. In the Dirac scotogenic model [21], additional scalars and fermionic fields are introduced along with the additional symmetry  $U(1)_{B-L} \times Z_2^{(A)} \times Z_2^{(B)}$ . The field content of this model, which is relevant to the lepton sector, and their charge assignments are given in Table I. Here, the symmetry  $U(1)_{B-L}$  can be either global or gauged [21]. In this work, we have taken this to be global, and it is an exact symmetry. With the charge assignments of Table I, the allowed interaction terms in the Lagrangian are

$$-\mathcal{L} = y_{\alpha\beta}(\nu_\alpha\phi^{+*} + \ell_\alpha\phi^{0*})\ell_\beta^c + f_{ak}(\nu_\alpha\eta^0 - \ell_\alpha\eta^+)N_k^c + h_{k\alpha}N_k\nu_\alpha^c\chi + m_{N_k}N_kN_k^c + \text{H.c.} \quad (1)$$

Here,  $m_{N_k}$  is the Dirac mass for  $N_k^D = (N_k, N_k^c)$ . The couplings  $y_{\alpha\beta}$  in Eq. (1) generate masses to charged leptons after the electroweak symmetry breaking, where  $\Phi$  acquires nonzero VEV. On the other hand, the terms of Eq. (1) do not generate masses to light neutrinos at tree level since  $\eta$  and  $\chi$  acquire zero VEVs, which is due to the fact that both these fields are charged under the exact symmetry  $Z_2^{(B)}$ . However, if there exists a trilinear term among  $\Phi$ ,  $\eta$ , and  $\chi$ , then neutrinos acquire masses at 1-loop level in this model. Shortly below, we explain how such a trilinear term can be present in this model. We notice from Table I that all the additional fields of this model are charged under the  $Z_2^{(B)}$  symmetry. Since this symmetry is exact, the lightest among

TABLE I. Fields in the lepton sector of the Dirac scotogenic model [21] along with their charge assignments. As described in Sec. I,  $\Phi$ ,  $\eta$ , and  $\chi$  are scalars. The rest of the fields are fermionic.

Field	$SU(2)_L$	$U(1)_Y$	$U(1)_{B-L}$	$Z_2^{(A)}$	$Z_2^{(B)}$
$L_\alpha = (\nu_\alpha, \ell_\alpha)$	2	-1/2	-1	+	+
$\ell_\alpha^c$	1	1	1	+	+
$\nu_\alpha^c$	1	0	1	-	+
$\Phi^T = (\phi^+, \phi^0)$	2	1/2	0	+	+
$\eta^T = (\eta^+, \eta^0)$	2	1/2	0	+	-
$\chi$	1	0	0	-	-
$N_k$	1	0	-1	+	-
$N_k^c$	1	0	1	+	-

these additional fields can be a candidate for dark matter. Later in this work, we discuss the possibility of a scalar dark matter in this model.

As discussed in the previous section, the Dirac scotogenic model is motivated from the scotogenic model [16], where neutrinos are Majorana particles. We notice that there is an analogy between these two models in terms of field content. Instead of  $(N_k, N_k^c)$ , there exists  $N_k^M$  in the scotogenic model, which is a Majorana field. The scalar sector of the scotogenic model is the same as that of the Dirac scotogenic model, except for the singlet field  $\chi$ . As a result of this, the third term of Eq. (1) does not exist in the Lagrangian of the scotogenic model. Moreover, by replacing  $(N_k, N_k^c)$  with a Majorana  $N_k^M$  field in Eq. (1), we get corresponding terms in the scotogenic model [16]. Later in this work, we compare the above two models in terms of neutrino masses and other physically observable quantities.

The scalar potential of the Dirac scotogenic model is [21]

$$V = \mu_1^2\Phi^\dagger\Phi + \mu_2^2\eta^\dagger\eta + \frac{1}{2}\mu_3^2\chi^2 + \frac{1}{2}\lambda_1(\Phi^\dagger\Phi)^2 + \frac{1}{2}\lambda_2(\eta^\dagger\eta)^2 + \lambda_3(\Phi^\dagger\Phi)(\eta^\dagger\eta) + \lambda_4(\Phi^\dagger\eta)(\eta^\dagger\Phi) + \frac{1}{2}[\lambda_5(\Phi^\dagger\eta)^2 + \text{H.c.}] + \frac{1}{4}\lambda_6\chi^4 + \frac{1}{2}\lambda_7(\Phi^\dagger\Phi)\chi^2 + \frac{1}{2}\lambda_8(\eta^\dagger\eta)\chi^2 + A\chi[\Phi^\dagger\eta + \text{H.c.}] \quad (2)$$

Here, we have chosen the parameter  $A$  to be real by fixing the phases in  $\Phi$  and  $\eta$ . For this particular choice, the parameter  $\lambda_5$  can, in general, be complex. However, in the analysis of [21],  $\lambda_5$  is taken to be real for the sake of simplicity. We discuss  $\lambda_5$  in the context of our work, later in the next section. The terms of Eq. (2) generate masses to physical fields of this model, after the electroweak symmetry breaking, where  $\Phi$  acquires nonzero VEV and the  $\eta$ ,  $\chi$  acquire zero VEVs. The nonzero VEV for  $\Phi$  can be taken as  $\langle\phi^0\rangle = v_{\text{EW}} = 174$  GeV, which is the electroweak symmetry breaking scale. We see that, after this symmetry breaking,  $\phi^+$  and imaginary part of  $\phi^0$  become Goldstone bosons. The real part of  $\phi^0$  is physical, and we identify  $\text{Re}(\phi^0) = H$  as the Higgs boson. The charged component of  $\eta$  is physical. On the other hand, the neutral component of  $\eta$  has mixing with  $\chi$  through the last term of Eq. (2). As a result of this, we write  $\eta^0 = (\eta_R^0 + i\eta_I^0)/\sqrt{2}$ . Now, the mass spectrum of the physical scalar fields in the Dirac scotogenic model is [21]

$$m_H^2 = 2\lambda_1 v_{\text{EW}}^2, \\ m_{\eta^\pm}^2 = \mu_2^2 + \lambda_3 v_{\text{EW}}^2, \\ m_{\eta^0}^2 \equiv m_{\chi^0}^2 = \mu_2^2 + (\lambda_3 + \lambda_4 - \lambda_5)v_{\text{EW}}^2, \\ M_{\eta_R^0, \chi}^2 = \begin{pmatrix} \mu_2^2 + (\lambda_3 + \lambda_4 + \lambda_5)v_{\text{EW}}^2 & \sqrt{2}Av_{\text{EW}} \\ \sqrt{2}Av_{\text{EW}} & \mu_3^2 + \lambda_7 v_{\text{EW}}^2 \end{pmatrix}. \quad (3)$$

Here,  $M_{\eta_R^0 \chi}^2$  gives the mixing masses between  $\eta_R^0$  and  $\chi$ , whose mass eigenstates are denoted by  $\zeta_{1,2}$ . Also here, for the sake of notational simplicity, we have written  $\eta_I^0 = \zeta_3$ .

The last term of Eq. (2) breaks the  $Z_2^{(A)}$  symmetry softly. This term is necessary in order to generate masses to neutrinos at 1-loop level [21], and moreover, this is the trilinear term that we have discussed above. Now, with the  $A$ -term of Eq. (2) and with the interaction terms of Eq. (1), neutrinos acquire masses at 1-loop, whose expressions are given below [21];

$$(\mathcal{M}_\nu)_{\alpha\beta} = (f\Lambda h)_{\alpha\beta} = \sum_{K=1}^3 f_{\alpha k} \Lambda_k h_{k\beta},$$

$$\Lambda_k = \frac{\sin(2\theta)}{32\pi^2 \sqrt{2}} m_{N_k}$$

$$\times \left[ \frac{m_{\zeta_1}^2}{m_{\zeta_1}^2 - m_{N_k}^2} \ln \frac{m_{\zeta_1}^2}{m_{N_k}^2} - \frac{m_{\zeta_2}^2}{m_{\zeta_2}^2 - m_{N_k}^2} \ln \frac{m_{\zeta_2}^2}{m_{N_k}^2} \right]. \quad (4)$$

Here,  $\theta$  is the mixing angle between  $\eta_R^0$  and  $\chi$ . As a result of this mixing, the diagonal masses for these fields are denoted by  $m_{\zeta_1}$  and  $m_{\zeta_2}$ . As already described before, this mixing is arising due to the  $A$ -term of Eq. (2). As a result of this,  $\theta$  is proportional to the  $A$  parameter. Since the  $A$ -term breaks  $Z_2^{(A)}$  symmetry softly, the parameter  $A$ , and hence, the  $\theta$  can be small. The small mass for neutrinos in Eq. (4) can be explained either through the small mixing angle  $\theta$ , or by the large value for  $m_{N_k}$ , or by taking degenerate masses for  $\zeta_{1,2}$ , apart from the loop suppression factor. It is to be noted that the masses of  $\zeta_{1,2}$  depend on various parameters, which are given in Eq. (3). It is possible to fine-tune these parameters in such way that  $m_{\zeta_1}$  and  $m_{\zeta_2}$  are nearly degenerate, which gives an additional suppression for neutrino masses in Eq. (4).

Apart from the smallness of neutrino masses, we need to explain the observed neutrino mixing angles [8] in the Dirac scotogenic model. In order to explain this, we use the Casas-Ibarra parametrization [29], and thereby, the Yukawa couplings in Eq. (4) can be expressed as

$$f = U \sqrt{m_\nu} R \sqrt{\Lambda}^{-1}, \quad h = \sqrt{\Lambda}^{-1} S^\dagger \sqrt{m_\nu} V^\dagger,$$

$$m_\nu = \text{diag}(m_{\nu_1}, m_{\nu_2}, m_{\nu_3}). \quad (5)$$

Here,  $m_{\nu_i}$ , where  $i = 1, 2, 3$ , are the neutrino mass eigenvalues.  $R$  and  $S$  are, in general, complex matrices, which satisfy  $RS^\dagger = I$ . After using the above parametrizations for  $f$  and  $h$  in Eq. (4), we get  $U^\dagger \mathcal{M}_\nu V = m_\nu$ , which is the desired relation for diagonalizing the  $\mathcal{M}_\nu$ . Here,  $U = U_{\text{PMNS}}$  is identified as the Pontecorvo-Maki-Nakagawa-Sakata matrix, which is parametrized in terms of the three neutrino mixing angles and a  $CP$  violating Dirac phase [8].  $V$  is a unitary matrix which rotates the right-handed neutrino fields from flavor to mass eigenstates. As a result

of the above given description, the neutrino mixing angles in the Dirac scotogenic model can be explained by parametrizing the Yukawa couplings as in Eq. (5). In the parametrizations of  $f$  and  $h$ , the neutrino mass eigenvalues can be chosen either in normal or inverted ordering, in order to fit the solar and atmospheric mass-square differences of neutrinos [8].

The expression for neutrino masses in the Dirac scotogenic model, which is given in Eq. (4), is similar to the corresponding expression of the scotogenic model [16]. In the context of neutrino mass generation, the difference between the above two models is described below. The neutrino masses in the Dirac scotogenic model are driven by two different Yukawa couplings, whereas, in the scotogenic model these masses are driven by one kind of Yukawa coupling. The parametrizations of Yukawa couplings in the Dirac scotogenic model, which are given in Eq. (5), are similar to that in the scotogenic model, which can be seen from [30]. In [30], we have worked on the lepton flavor violating (LFV) decays of  $Z$  and Higgs boson in the scotogenic model, where we have also done numerical analysis on fitting the neutrino masses and mixing angles in this model. This numerical analysis can be analogously worked in the Dirac scotogenic model.

To test the Dirac scotogenic model in collider experiments, such as the LHC, we should take the masses of all additional fields to be around a few hundred GeV. Now, using the discussion given before, for  $m_{N_k} \sim 1$  TeV, the small masses for neutrinos can be explained if either of the following quantities are taken to be small:  $\theta$  or  $m_{\zeta_1} - m_{\zeta_2}$ . In the limit that these quantities are small, we see that  $\Lambda_k$  of Eq. (4) becomes small. Hence, from Eq. (5), the Yukawa couplings  $f$  and  $h$  can become  $\mathcal{O}(1)$  in some region of parameter space. The couplings  $f_{\alpha k}$  drive LFV processes in this model, which can have significant branching ratios, since  $f_{\alpha k}$  are not suppressed and  $m_{N_k} \sim 1$  TeV. Later in this work, we describe about LFV processes of this model.

As described before, in the Dirac scotogenic model,  $\Phi$  acquires nonzero VEV and  $\eta, \chi$  should acquire zero VEVs. This pattern of VEVs can be achieved by minimizing the potential of Eq. (2) for  $\mu_1^2 < 0$ . Here we notice that in some parameter region of the scalar potential the above pattern of VEVs constitutes a minimum for the model. By choosing different parameter regions of the scalar potential, it is possible to find other minima of this model. In the next section, we argue that the above minimum required for the Dirac scotogenic model is only one possible minima of this model.

### III. POSSIBLE MINIMA OF THE DIRAC SCOTOGENIC MODEL

In this section, we describe different possible minima of the Dirac scotogenic model, after analyzing the scalar potential of it. The scalar potential of this model is described in Eq. (2), which consists of the fields  $\Phi, \eta$

and,  $\chi$ . At the minimum of the scalar potential, either of these scalar fields can acquire nonzero VEVs. First, let us consider the case where  $\langle\Phi\rangle \neq 0$  and  $\langle\eta\rangle = 0$ . In this case, using the  $SU(2)$  transformation, the VEV of  $\Phi$  can always be brought into a form where the neutral component of it acquires nonzero and real VEV. As a result of this, there can exist two different minima, depending on whether  $\chi$  acquires a VEV or not. These possible minima are

$$N1: \langle\Phi\rangle = \begin{pmatrix} 0 \\ v_{EW} \end{pmatrix}, \quad \langle\eta\rangle = \begin{pmatrix} 0 \\ 0 \end{pmatrix}, \quad \langle\chi\rangle = 0. \quad (6)$$

$$N2: \langle\Phi\rangle = \begin{pmatrix} 0 \\ v_{\phi(2)} \end{pmatrix}, \quad \langle\eta\rangle = \begin{pmatrix} 0 \\ 0 \end{pmatrix}, \quad \langle\chi\rangle = v_{\chi(2)}, \quad (7)$$

where  $v_{\phi(2)}$  and  $v_{\chi(2)}$  are some nonzero real variables. Here,  $N1, N2$  are neutral minima which break only the electro-weak symmetry.  $N1$  is the desired minimum of the Dirac scotogenic model, which we have considered to be the true model of our Universe. Hence, we have equated the VEV of  $\Phi$  field to  $v_{EW}$ . On the other hand,  $N2$  is one possible minima of the scalar potential of the Dirac scotogenic model. But otherwise, this minimum is not consistent with the model framework. Hence,  $N2$  does not represent the observable world of our Universe. As a result of this, the VEVs of  $\Phi$  and  $\chi$  in this minimum are some variables and need not represent the electroweak symmetry breaking scale. Now, let us consider the case where  $\langle\Phi\rangle = 0$  and  $\langle\eta\rangle \neq 0$ . In this case, in analogy to the description given above, the following two minima are possible:

$$N3: \langle\Phi\rangle = \begin{pmatrix} 0 \\ 0 \end{pmatrix}, \quad \langle\eta\rangle = \begin{pmatrix} 0 \\ v_{\eta(3)} \end{pmatrix}, \quad \langle\chi\rangle = 0. \quad (8)$$

$$N4: \langle\Phi\rangle = \begin{pmatrix} 0 \\ 0 \end{pmatrix}, \quad \langle\eta\rangle = \begin{pmatrix} 0 \\ v_{\eta(4)} \end{pmatrix}, \quad \langle\chi\rangle = v_{\chi(4)}. \quad (9)$$

The nonzero entries in the above equations are real and arbitrary. The minima  $N3$  and  $N4$  are unphysical since they do not generate masses to SM fermions of this model.

In the case where  $\langle\Phi\rangle = 0 = \langle\eta\rangle$ , there can exist one nontrivial minimum, which is given below,

$$N5: \langle\Phi\rangle = \begin{pmatrix} 0 \\ 0 \end{pmatrix}, \quad \langle\eta\rangle = \begin{pmatrix} 0 \\ 0 \end{pmatrix}, \quad \langle\chi\rangle = v_{\chi(5)}. \quad (10)$$

Here, the VEV of  $\chi$  is real and a nonzero variable. The minimum  $N5$  is clearly unphysical since it does not break the electroweak symmetry. Finally, in the case where  $\langle\Phi\rangle \neq 0 \neq \langle\eta\rangle$ , the following six minima are possible:

$$N6: \langle\Phi\rangle = \begin{pmatrix} 0 \\ v_{\phi(6)} \end{pmatrix}, \quad \langle\eta\rangle = \begin{pmatrix} 0 \\ v_{\eta(6)} \end{pmatrix}, \quad \langle\chi\rangle = 0. \quad (11)$$

$$N7: \langle\Phi\rangle = \begin{pmatrix} 0 \\ v_{\phi(7)} \end{pmatrix}, \quad \langle\eta\rangle = \begin{pmatrix} 0 \\ iv_{\eta(7)} \end{pmatrix}, \quad \langle\chi\rangle = 0. \quad (12)$$

$$N8: \langle\Phi\rangle = \begin{pmatrix} 0 \\ v_{\phi(8)} \end{pmatrix}, \quad \langle\eta\rangle = \begin{pmatrix} 0 \\ v_{\eta(8)} \end{pmatrix}, \quad \langle\chi\rangle = v_{\chi(8)}. \quad (13)$$

$$C9: \langle\Phi\rangle = \begin{pmatrix} 0 \\ v_{\phi(9)} \end{pmatrix}, \quad \langle\eta\rangle = \begin{pmatrix} c_{\eta(9)} \\ v_{\eta(9)} \end{pmatrix}, \quad \langle\chi\rangle = 0. \quad (14)$$

$$C10: \langle\Phi\rangle = \begin{pmatrix} 0 \\ v_{\phi(10)} \end{pmatrix}, \quad \langle\eta\rangle = \begin{pmatrix} c_{\eta(10)} \\ iv_{\eta(10)} \end{pmatrix}, \quad \langle\chi\rangle = 0. \quad (15)$$

$$C11: \langle\Phi\rangle = \begin{pmatrix} 0 \\ v_{\phi(11)} \end{pmatrix}, \quad \langle\eta\rangle = \begin{pmatrix} c_{\eta(11)} \\ v_{\eta(11)} \end{pmatrix}, \quad \langle\chi\rangle = v_{\chi(11)}. \quad (16)$$

Here,  $C9, C10$ , and  $C11$  are charge-breaking minima, where the charged component of  $\eta$  acquires nonzero VEV. On the other hand,  $N6, N7$ , and  $N8$  break only the electroweak symmetry. In obtaining the forms of VEVs in Eqs. (11)–(16), we have used the  $SU(2)$  transformation [31] on  $\Phi$  and  $\eta$ . It is to be noticed that the variables of the form  $v_{\phi(k)}, v_{\eta(k)}, c_{\eta(k)}, v_{\chi(k)}$  in Eqs. (11)–(16) are real and nonzero. While obtaining that these variables are real, we have taken the  $\lambda_5$  parameter of Eq. (2) to be real. Shortly below, we give a demonstration about this. We notice that the VEV of  $\eta$  in Eqs. (12) and (15) is complex, which tells something about  $CP$  symmetry in the minima of  $N7$  and  $C10$ . As we have taken  $\lambda_5$  to be real, the minimum  $N7$  respect the  $CP$  symmetry, since Eqs. (2) and (12) are invariant under the following  $CP$  transformation:  $\Phi \rightarrow \Phi^*, \eta \rightarrow -\eta^*, \chi \rightarrow -\chi$ . On the other hand,  $C10$  breaks the  $CP$  symmetry spontaneously, apart from the charge and electroweak symmetries.

After using the  $SU(2)$  transformation [31], the general structure of the VEVs of the scalar fields in the Dirac scotogenic model can be written as

$$\langle\Phi\rangle = \begin{pmatrix} 0 \\ v_{\phi} \end{pmatrix}, \quad \langle\eta\rangle = \begin{pmatrix} c_{\eta} \\ v_{\eta} \end{pmatrix}, \quad \langle\chi\rangle = v_{\chi}. \quad (17)$$

In the above equation,  $v_{\phi}, c_{\eta}, v_{\chi}$  are real variables, and  $v_{\eta}$  is, in general, a complex variable. Apart from  $v_{\eta}$ , the other complex variable in this model is the  $\lambda_5$  parameter of Eq. (2). As a result of this, we write the forms for  $\lambda_5$  and  $v_{\eta}$  as

$$\lambda_5 = |\lambda_5|e^{i\theta_5}, \quad v_{\eta} = |v_{\eta}|e^{i\theta_{\eta}}. \quad (18)$$

Here,  $\theta_5$  and  $\theta_{\eta}$  are phases in  $\lambda_5$  and  $v_{\eta}$ , respectively. After plugging Eq. (17) into Eq. (2), the relevant part of the potential is

$$\langle V \rangle = |\lambda_5|v_\phi^2|v_\eta|^2 \cos(\theta_5 + 2\theta_\eta) + 2Av_\chi v_\phi |v_\eta| \cos \theta_\eta. \quad (19)$$

In the above equation, we have written only that part of the potential which contains only the phases  $\theta_5$  and  $\theta_\eta$ . The extremum for  $\langle V \rangle$  with respect to these phases is found to be

$$\theta_5 = (m - 2n)\pi, \quad \theta_\eta = n\pi. \quad (20)$$

Here,  $m, n$  are any integers. Using the above relations, we see that  $\lambda_5$  and  $v_\eta$  are real quantities at any extremum of the potential. To see if the values of Eq. (20) correspond to the minimum of Eq. (19), we need to evaluate the second-order derivatives of  $\langle V \rangle$  with respect to  $\theta_5$  and  $\theta_\eta$ . As a result of this, we get the following matrix:

$$M_V = \begin{pmatrix} \frac{\partial^2 \langle V \rangle}{\partial \theta_5^2} & \frac{\partial^2 \langle V \rangle}{\partial \theta_5 \partial \theta_\eta} \\ \frac{\partial^2 \langle V \rangle}{\partial \theta_5 \partial \theta_\eta} & \frac{\partial^2 \langle V \rangle}{\partial \theta_\eta^2} \end{pmatrix} \Bigg|_{\theta_5=(m-2n)\pi, \theta_\eta=n\pi}. \quad (21)$$

After demanding that the eigenvalues of  $M_V$  are positive, and since  $\lambda_5$  and  $v_\eta$  are real at the minimum of the potential, we get the following conditions:

$$\lambda_5 < 0, \quad Av_\phi v_\eta v_\chi < 0. \quad (22)$$

Using the analysis, which is described in the previous paragraph, we notice that in the minima of Eqs. (13) and (16), the quantities  $v_{\eta(8)}$  and  $v_{\eta(11)}$  should be real. Moreover, in these minima,  $\lambda_5$  should be a real parameter, and the conditions of Eq. (22) should be satisfied. Now, in the analysis of the previous paragraph, let us consider the case where  $v_\chi = 0$ . In this case, at the minimum of the

potential, the individual phases in  $\lambda_5$  and  $v_\eta$  cannot be determined. However, if we choose  $\lambda_5$  to be real, then  $v_\eta$  can be either real or purely imaginary at the minimum of the potential. As a result of this, the VEV of the neutral component of  $\eta$  is taken to be real in Eqs. (11) and (14), whereas, this quantity is taken to be purely imaginary in Eqs. (12) and (15). Let us mention here that  $\lambda_5$  can, in general, be complex in the minima of Eqs. (6)–(10). However, to simplify our numerical analysis, we have taken  $\lambda_5$  to be real in the rest of this work.

We have described that the VEV structures given in Eqs. (6)–(16) as possible minima of the model. In order to clarify this point, we refer each of these VEV structures as a stationary point (SP). A SP becomes a minimum if the following two conditions are satisfied: (1) minimization conditions of the scalar potential, (2) mass-square eigenvalues of scalar fields, which are not Goldstone bosons, are positive. The minimization conditions, which should be satisfied by the SPs of Eqs. (6)–(16), are given in Table II. Shortly below, we describe how we compute the mass-square eigenvalues of scalar fields at the SPs of Eqs. (6)–(16). It is to be noted that, in the Dirac scotogenic model, the scalar sector consists of nine real degrees of freedom. Out of these nine, some of them may become Goldstone bosons since the electroweak and charge symmetries are spontaneously broken by some of the SPs of Eqs. (6)–(16). The SP  $N5$  of Eq. (10) does not break either of these symmetries, and hence, in this case all the nine scalar fields become massive.

As stated before, the general structure of VEVs of scalar fields in the Dirac scotogenic model is given by Eq. (17). Hence, in order to compute the mass eigenstates, we parametrize these fields as

TABLE II. Minimization conditions which should be satisfied at the SPs of Eqs. (6)–(16).

N1	$\mu_1^2 + \lambda_1 v_{\text{EW}}^2 = 0$
N2	$A = 0, \mu_1^2 + \lambda_1 v_{\phi(2)}^2 + \frac{1}{2}\lambda_7 v_{\chi(2)}^2 = 0, \mu_3^2 + \lambda_6 v_{\chi(2)}^2 + \lambda_7 v_{\phi(2)}^2 = 0$
N3	$\mu_2^2 + \lambda_2 v_{\eta(3)}^2 = 0$
N4	$A = 0, \mu_2^2 + \lambda_2 v_{\eta(4)}^2 + \frac{1}{2}\lambda_8 v_{\chi(4)}^2 = 0, \mu_3^2 + \lambda_6 v_{\chi(4)}^2 + \lambda_8 v_{\eta(4)}^2 = 0$
N5	$\mu_3^2 + \lambda_6 v_{\chi(5)}^2 = 0$
N6	$A = 0, \mu_1^2 + \lambda_1 v_{\phi(6)}^2 + (\lambda_3 + \lambda_4 + \lambda_5)v_{\eta(6)}^2 = 0, \mu_2^2 + \lambda_2 v_{\eta(6)}^2 + (\lambda_3 + \lambda_4 + \lambda_5)v_{\phi(6)}^2 = 0$
N7	$\mu_1^2 + \lambda_1 v_{\phi(7)}^2 + (\lambda_3 + \lambda_4 - \lambda_5)v_{\eta(7)}^2 = 0, \mu_2^2 + \lambda_2 v_{\eta(7)}^2 + (\lambda_3 + \lambda_4 - \lambda_5)v_{\phi(7)}^2 = 0$
N8	$\mu_1^2 + \lambda_1 v_{\phi(8)}^2 + (\lambda_3 + \lambda_4 + \lambda_5)v_{\eta(8)}^2 + \frac{1}{2}\lambda_7 v_{\chi(8)}^2 + Av_{\chi(8)}v_{\eta(8)}/v_{\phi(8)} = 0,$ $\mu_2^2 + \lambda_2 v_{\eta(8)}^2 + (\lambda_3 + \lambda_4 + \lambda_5)v_{\phi(8)}^2 + \frac{1}{2}\lambda_8 v_{\chi(8)}^2 + Av_{\chi(8)}v_{\phi(8)}/v_{\eta(8)} = 0,$ $\mu_3^2 + \lambda_6 v_{\chi(8)}^2 + \lambda_7 v_{\phi(8)}^2 + \lambda_8 v_{\eta(8)}^2 + 2Av_{\phi(8)}v_{\eta(8)}/v_{\chi(8)} = 0$
C9	$A = 0, \lambda_4 + \lambda_5 = 0, \mu_1^2 + \lambda_1 v_{\phi(9)}^2 + \lambda_3(c_{\eta(9)}^2 + v_{\eta(9)}^2) = 0, \mu_2^2 + \lambda_2(c_{\eta(9)}^2 + v_{\eta(9)}^2) + \lambda_3 v_{\phi(9)}^2 = 0$
C10	$\lambda_4 - \lambda_5 = 0, \mu_1^2 + \lambda_1 v_{\phi(10)}^2 + \lambda_3(c_{\eta(10)}^2 + v_{\eta(10)}^2) = 0, \mu_2^2 + \lambda_2(c_{\eta(10)}^2 + v_{\eta(10)}^2) + \lambda_3 v_{\phi(10)}^2 = 0$
C11	$Av_{\chi(11)} + (\lambda_4 + \lambda_5)v_{\eta(11)}v_{\phi(11)} = 0, \mu_1^2 + \lambda_1 v_{\phi(11)}^2 + \lambda_3(c_{\eta(11)}^2 + v_{\eta(11)}^2) + \frac{1}{2}\lambda_7 v_{\chi(11)}^2 = 0,$ $\mu_2^2 + \lambda_2(c_{\eta(11)}^2 + v_{\eta(11)}^2) + \lambda_3 v_{\phi(11)}^2 + \frac{1}{2}\lambda_8 v_{\chi(11)}^2 = 0,$ $\mu_3^2 + \lambda_6 v_{\chi(11)}^2 + \lambda_7 v_{\phi(11)}^2 + \lambda_8(c_{\eta(11)}^2 + v_{\eta(11)}^2) + 2Av_{\phi(11)}v_{\eta(11)}/v_{\chi(11)} = 0$

$$\begin{aligned}
\Phi &= \begin{pmatrix} (\phi_R^1 + i\phi_I^1)/\sqrt{2} \\ v_\phi + (\phi_R^0 + i\phi_I^0)/\sqrt{2} \end{pmatrix}, \\
\eta &= \begin{pmatrix} c_\eta + (\eta_R^1 + i\eta_I^1)/\sqrt{2} \\ v_\eta + (\eta_R^0 + i\eta_I^0)/\sqrt{2} \end{pmatrix}, \\
\chi &= v_\chi + \chi_R.
\end{aligned} \tag{23}$$

Now, in the case of Eq. (6), which corresponds to the desired minimum of the Dirac scotogenic model,  $\phi_R^1, \phi_I^1, \phi_I^0$  become Goldstone bosons. Moreover, for this minimum, we have  $v_\phi = v_{EW}$  and  $c_\eta = v_\eta = v_\chi = 0$ . Now, after identifying  $\phi_R^0 = H$  as the Higgs boson and  $\eta^+ = (\eta_R^1 + i\eta_I^1)/\sqrt{2}$ , we see that the mass spectrum of physical fields in the case of  $N1$  matches with that of Eq. (3). Similar to what we described above, the mass spectrum of scalar fields at other SPs of Eqs. (7)–(16) are computed accordingly. It should be noted here that, even if any of these SPs become minima, the scalar fields in these minima are unphysical since these minima do not represent the physical world of ours. In our analysis, which we will present later, we have computed the scalar masses at the SPs of Eqs. (7)–(16) numerically. We have found in our analysis that each of the SPs given in Eqs. (6)–(16) can become a minimum in some region of parameter space of the scalar potential. Since multiple minima can exist for the scalar potential of the Dirac scotogenic model, we need to know if  $N1$ , which is the desired minimum of this model, can become the global minimum. The next few sections discuss this.

#### IV. RELATIVE DEPTHS IN POTENTIAL

At the end of the last section, we noted that  $N1$  is one possible minimum among other minima of the Dirac scotogenic model. In order to address if  $N1$  is the global minimum of this model, we need to know if  $N1$  coexists with other minima. If it coexist with other minima, we demand that the potential depth at  $N1$  is lower compared to that at other minima, so that  $N1$  is the global minimum of this model. In this section, we assume that the minimum  $N1$  coexists with other minima in some region of parameter space. We then calculate the differences in the depth of potential at  $N1$  and at other minima. Using these quantities, we predict the possibility of making  $N1$  the global minimum of this model. The results obtained in this section are helpful for the next section, where we study the coexistence of  $N1$  with other minima.

In order to compute the difference between the value of potential at  $N1$  and at any other SP, we follow the work of [12,13,32], which is based on a formalism of bilinears. For some works using the bilinear formalism, see Refs. [33–37]. Using this formalism, we notice that, except for the last term of Eq. (2), other terms of the scalar

potential are either quadratic or quartic. As a result of this, we define the following bilinears:

$$\begin{aligned}
x_1 &= \Phi^\dagger \Phi, & x_2 &= \eta^\dagger \eta, & x_3 &= \chi^2, \\
x_4 &= \text{Re}(\Phi^\dagger \eta), & x_5 &= \text{Im}(\Phi^\dagger \eta).
\end{aligned} \tag{24}$$

Apart from these, we also define the following matrices:

$$\begin{aligned}
X &= \begin{pmatrix} x_1 \\ x_2 \\ x_3 \\ x_4 \\ x_5 \end{pmatrix}, & M_2 &= \begin{pmatrix} \mu_1^2 \\ \mu_2^2 \\ \frac{1}{2}\mu_3^2 \\ 0 \\ 0 \end{pmatrix}, \\
M_4 &= \begin{pmatrix} \lambda_1 & \lambda_3 & \frac{1}{2}\lambda_7 & 0 & 0 \\ \lambda_3 & \lambda_2 & \frac{1}{2}\lambda_8 & 0 & 0 \\ \frac{1}{2}\lambda_7 & \frac{1}{2}\lambda_8 & \frac{1}{2}\lambda_6 & 0 & 0 \\ 0 & 0 & 0 & 2(\lambda_4 + \lambda_5) & 0 \\ 0 & 0 & 0 & 0 & 2(\lambda_4 - \lambda_5) \end{pmatrix}.
\end{aligned} \tag{25}$$

Now, using Eqs. (24) and (25), the scalar potential of Eq. (2) can be expressed as

$$\begin{aligned}
V &= V_2 + V_3 + V_4, \\
V_2 &= M_2^T X, & V_3 &= 2A\chi x_4, & V_4 &= \frac{1}{2}X^T M_4 X.
\end{aligned} \tag{26}$$

At any SP of Eqs. (6)–(16), the scalar potential has to satisfy the minimization conditions. Hence, we get the following relation [32]:

$$\sum_i \varphi_i \left. \frac{\partial V}{\partial \varphi_i} \right|_{\text{SP}} = 0 \Rightarrow 2(V_2)_{\text{SP}} + 3(V_3)_{\text{SP}} + 4(V_4)_{\text{SP}} = 0. \tag{27}$$

In the above equation,  $\varphi_i$  represent any real scalar degree of freedom of the Dirac scotogenic model. Here,  $(V_i)_{\text{SP}}$ , where  $i = 2, 3, 4$ , is the value of  $V_i$  evaluated at a SP. Using the above relation, the value of scalar potential evaluated at a SP is found to be

$$V_{\text{SP}} = \frac{1}{2}(V_2)_{\text{SP}} + \frac{1}{4}(V_3)_{\text{SP}}. \tag{28}$$

We define  $X_{\text{SP}}$  as the matrix  $X$  evaluated at a SP. We then define the following quantity at any SP:

$$V'_{\text{SP}} = M_2 + M_4 X_{\text{SP}}. \tag{29}$$

Using the above definitions, for the case of  $N1$ , we get

$$X_{N1} = \begin{pmatrix} v_{\text{EW}}^2 \\ 0 \\ 0 \\ 0 \\ 0 \end{pmatrix}, \quad V'_{N1} = \begin{pmatrix} 0 \\ m_{\eta^+}^2 \\ \frac{1}{2}(\mu_3^2 + \lambda_7 v_{\text{EW}}^2) \\ 0 \\ 0 \end{pmatrix}. \quad (30)$$

While obtaining the form of  $V'_{N1}$ , we have used the minimization condition for  $N1$ , which is given in Table II. Similarly, for other SPs of Eqs. (7)–(16), we have obtained  $X_{\text{SP}}$  and  $V'_{\text{SP}}$ , accordingly. Below we describe the expression for difference in the value of potential at  $N1$  and at any other SP. To do this computation, we first consider the following products:  $X_{N1}^T V'_{\text{SP}}$  and  $X_{\text{SP}}^T V'_{N1}$ . Now, using the quantities described in the previous paragraph, these products can be expressed as

$$\begin{aligned} X_{N1}^T V'_{\text{SP}} &= 2V_{N1} - \frac{1}{2}(V_3)_{N1} + X_{N1}^T M_4 X_{\text{SP}}, \\ X_{\text{SP}}^T V'_{N1} &= 2V_{\text{SP}} - \frac{1}{2}(V_3)_{\text{SP}} + X_{\text{SP}}^T M_4 X_{N1}. \end{aligned} \quad (31)$$

From the relations in the above equation, we get the following expression, which gives the relative depth in potential between a SP and  $N1$ ,

$$V_{\text{SP}} - V_{N1} = \frac{1}{2}(X_{\text{SP}}^T V'_{N1} - X_{N1}^T V'_{\text{SP}}) + \frac{1}{4}((V_3)_{\text{SP}} - (V_3)_{N1}). \quad (32)$$

It is to remind here that the above expression is obtained after using the minimization conditions for the SPs of Eqs. (6)–(16), but otherwise, these SPs need not be minima.

Using the general expression given in Eq. (32), we have computed the differences in the value of potential at  $N1$  and at any other SP of Eqs. (7)–(16). These expressions are given below,

$$V_{N2} - V_{N1} = \frac{v_{\chi(2)}^2}{4}(\mu_3^2 + \lambda_7 v_{\text{EW}}^2), \quad (33)$$

$$V_{N3} - V_{N1} = \frac{v_{\eta(3)}^2}{2}\mu_2^2 - \frac{v_{\text{EW}}^2}{2}\mu_1^2, \quad (34)$$

$$V_{N4} - V_{N1} = \frac{v_{\eta(4)}^2}{2}\mu_2^2 - \frac{v_{\text{EW}}^2}{2}\mu_1^2 + \frac{v_{\chi(4)}^2}{4}\mu_3^2, \quad (35)$$

$$V_{N5} - V_{N1} = \frac{v_{\chi(5)}^2}{4}\mu_3^2 - \frac{v_{\text{EW}}^2}{2}\mu_1^2, \quad (36)$$

$$V_{N6} - V_{N1} = \frac{v_{\eta(6)}^2}{2}(\mu_2^2 + (\lambda_3 + \lambda_4 + \lambda_5)v_{\text{EW}}^2), \quad (37)$$

$$V_{N7} - V_{N1} = \frac{v_{\eta(7)}^2}{2}m_{\eta^0}^2, \quad (38)$$

$$\begin{aligned} V_{N8} - V_{N1} &= \frac{v_{\eta(8)}^2}{2}(\mu_2^2 + (\lambda_3 + \lambda_4 + \lambda_5)v_{\text{EW}}^2) \\ &\quad + \frac{v_{\chi(8)}^2}{4}(\mu_3^2 + \lambda_7 v_{\text{EW}}^2) \\ &\quad + \frac{A v_{\chi(8)} v_{\eta(8)}}{2v_{\phi(8)}}(v_{\text{EW}}^2 + v_{\phi(8)}^2), \end{aligned} \quad (39)$$

$$V_{C9} - V_{N1} = \frac{c_{\eta(9)}^2 + v_{\eta(9)}^2}{2}m_{\eta^+}^2, \quad (40)$$

$$V_{C10} - V_{N1} = \frac{c_{\eta(10)}^2 + v_{\eta(10)}^2}{2}m_{\eta^+}^2, \quad (41)$$

$$\begin{aligned} V_{C11} - V_{N1} &= \frac{c_{\eta(11)}^2 + v_{\eta(11)}^2}{2}m_{\eta^+}^2 + \frac{v_{\chi(11)}^2}{4}(\mu_3^2 + \lambda_7 v_{\text{EW}}^2) \\ &\quad + \frac{1}{2}A v_{\chi(11)} v_{\eta(11)} v_{\phi(11)}. \end{aligned} \quad (42)$$

In the above equations,  $m_{\eta^+}^2$  and  $m_{\eta^0}^2$  are mass-square eigenvalues of  $\eta^+$  and  $\eta^0$  for  $N1$ , whose expressions are given in Eq. (3). Now, in the region where  $N1$  is a minimum, we should have  $m_{\eta^+}^2 > 0$  and  $m_{\eta^0}^2 > 0$ . Hence, in this region, we get  $V_{N7} - V_{N1} > 0$ ,  $V_{C9} - V_{N1} > 0$ , and  $V_{C10} - V_{N1} > 0$ . This means, if the  $N1$  minimum coexist with either of  $N7$ ,  $C9$ , and  $C10$ , then the value of potential at  $N1$  is always lower than that at  $N7$ ,  $C9$ , and  $C10$ . Now, let us consider a region where the  $N1$  minimum coexists with either  $N2$  or  $N6$ . In this region, we should have  $A = 0$  since this is one of the minimization conditions for  $N2$  and  $N6$ , which can be seen from Table II. Now, using  $A = 0$  in Eq. (3) and also from the fact that  $N1$  is a minimum, we get  $\mu_2^2 + (\lambda_3 + \lambda_4 + \lambda_5)v_{\text{EW}}^2 > 0$  and  $\mu_3^2 + \lambda_7 v_{\text{EW}}^2 > 0$ . This implies  $V_{N2} - V_{N1} > 0$  and  $V_{N6} - V_{N1} > 0$ , which means that the potential depth at  $N1$  is deeper than that at  $N2$  and  $N6$ .

We have argued above that the potential value at  $N1$  is always lower than that at  $N2$ ,  $N6$ ,  $N7$ ,  $C9$ , and  $C10$  in a region where these minima coexist. However, the situation is different in a region where the  $N1$  minimum coexists with either of  $N3$ ,  $N4$ , and  $N5$ . In each of Eqs. (34)–(36), there exist both positive and negative terms, and hence, it is not guaranteed that the potential depth at  $N1$  is deeper than that at  $N3$ ,  $N4$ , and  $N5$ . Now, let us look at Eqs. (39) and (42), which give the relative potential depths for  $N8$  and  $C11$  with  $N1$ . As described in Sec. III, the minima  $N8$  and  $C11$  should satisfy the conditions of Eq. (22). As a result of this, the last term of Eqs. (39) and (42) should give negative contribution. Hence, it is not guaranteed that the potential depth at  $N1$  is lower than that at  $N8$  and  $C11$ .

In Sec. III, we have described that 11 different minima can exist in the Dirac scotogenic model. If we assume that  $N1$ , which is the desired minimum of this model, coexists

with other minima of this model, then we have shown that the potential value at  $N1$  is not guaranteed to be deeper than that at  $N3$ ,  $N4$ ,  $N5$ ,  $N8$ , and  $C11$ . But otherwise, we have argued that  $N1$  minimum is stable against the other vacua of  $N2$ ,  $N6$ ,  $N7$ ,  $C9$ , and  $C10$ . Now, in order to address if  $N1$  can be made the global minimum of this model, we follow the below described steps. First, we find a parameter region of this model where  $N1$  is a minimum. Now in this parameter region, we check if  $N1$  coexists with either of the minima of  $N3$ ,  $N4$ ,  $N5$ ,  $N8$ , and  $C11$ . If  $N1$  minimum is found to coexist with the above described minima, then we demand that the relative potential depths for these minima against  $N1$ , which are given in Eqs. (34), (35), (36), (39), and (42), should be positive. After this demand, we see that  $N1$  becomes the global minimum in the region of coexistence. In the next section, we present numerical analysis on the above described steps and give results on the status of  $N1$  as the global minimum of this model.

## V. NUMERICAL RESULTS

As we have described at the end of the last section, we first find a parameter region where  $N1$  is a minimum and then check if  $N1$  coexists with the other minima of  $N3$ ,  $N4$ ,  $N5$ ,  $N8$ , and  $C11$  in this region. This parameter region depends on the dimensionless  $\lambda$  parameters and dimensionful parameters of the scalar potential, which is given in Eq. (2). While finding the above mentioned parameter region, we scan over these parameters in such a way that perturbativity bounds on  $\lambda$  parameters and boundedness from below conditions on the scalar potential are satisfied. As a result of this, in our scan over parameters, the below perturbativity conditions are satisfied on  $\lambda$  parameters,

$$|\lambda_i| \leq 4\pi. \quad (43)$$

As for the boundedness from below conditions, they are determined by the quartic part of the scalar potential. In our case, the quartic part of the scalar potential is the same as that considered in [38]. Hence, the allowed region by the boundedness from below of the scalar potential of the Dirac scotogenic model is given by [38]

$$\begin{aligned} &\Omega_1 \cup \Omega_2, \\ &\Omega_1 = \left\{ \lambda_{1,2,6} > 0; \sqrt{2\lambda_1\lambda_6} + \lambda_7 > 0; \sqrt{2\lambda_2\lambda_6} + \lambda_8 > 0; \right. \\ &\quad \left. \sqrt{\lambda_1\lambda_2} + \lambda_3 + D > 0; \lambda_7 + \sqrt{\frac{\lambda_1}{\lambda_2}}\lambda_8 \geq 0 \right\}, \\ &\Omega_2 = \{ \lambda_{1,2,6} > 0; 2\lambda_2\lambda_6 \geq \lambda_8^2; \sqrt{2\lambda_1\lambda_6} > -\lambda_7 \geq \sqrt{2\lambda_2\lambda_6} + \lambda_8; \\ &\quad \sqrt{(\lambda_7^2 - 2\lambda_1\lambda_6)(\lambda_8^2 - 2\lambda_2\lambda_6)} > \lambda_7\lambda_8 - 2(D + \lambda_3)\lambda_6 \}, \\ &D = \min(\lambda_4 - |\lambda_5|, 0). \end{aligned} \quad (44)$$

In our numerical analysis, we randomly generate the  $\lambda$  parameters in such a way that the bounds in Eqs. (43) and (44) are satisfied. In addition to these  $\lambda$  parameters, dimensionful parameters are also existent in the scalar potential of Eq. (2). Among these dimensionful parameters, we fix  $\mu_1^2 = -\lambda_1 v_{\text{EW}}^2$  in our numerical analysis. This is due to the fact that we search for a region where  $N1$  is a minimum, and the above relation is the minimization condition for this minimum. The rest of the dimensionful parameters such as  $\mu_2^2, \mu_3^2, A$  are either fixed to a value or randomly generated. Here, we notice that the  $A$ -parameter is necessary in order to explain neutrino masses in the Dirac scotogenic model, which we have discussed in Sec. II. It is described that this parameter breaks  $Z_2^{(A)}$  symmetry softly, and hence, this parameter should be small. As a result of this, we have taken this parameter to be small in our numerical analysis. On the other hand, the parameters  $\mu_{2,3}^2$ , except that for  $N1$ , determine the minimization conditions of all minima, which can be seen from Table II. As a result of this, either we have fixed these parameters in order to satisfy minimization conditions of a particular minimum, or else, we have generated them randomly. We discuss details on these parameters later.

In the previous paragraph, we have described our methodology in scanning over parameters of the scalar potential. We notice that these parameters are physical since they can be measured in future experiments. Apart from these parameters, in our scanning procedure, we have randomly varied the nonzero VEVs of Eqs. (7)–(16). It is to remind here that the minima of Eqs. (7)–(16) are unphysical since they do not correspond to the vacuum of our physical world. As a result of this, the nonzero VEVs of Eqs. (7)–(16) are unknown, and *a priori*, they can take arbitrary values.

As described previously, we scan over parameters of the model and find a region where  $N1$  is a minimum. For the  $N1$  minimum, the mass eigenstates of the scalar fields are physical since this minimum corresponds to the vacuum of our physical world. The mass eigenstates of this minimum are described in Eq. (3). Among these eigenstates, only the Higgs boson is found in the LHC experiment and rest of the scalar fields are yet to be found. In order to fit the Higgs boson mass in our analysis, we have taken  $m_H = 125.25$  GeV [8]. This value of Higgs boson mass also fixes the  $\lambda_1$  parameter in our analysis. Regarding the additional mass eigenstates of the  $N1$  minimum, they should satisfy the phenomenological lower bounds on their masses due to nonobservation of these fields in collider experiments. As a result of this, we apply the following bounds on these masses in our analysis:

$$m_{\eta^+} > 105 \text{ GeV}, \quad m_{\zeta_{1,2,3}} > 5 \text{ GeV}. \quad (45)$$

The lower bound of 105 GeV on  $m_{\eta^+}$  is based on the fact that no non-SM charged particle is found in the large electron positron collider.

Below we present our numerical results in the form of percentage of chances on the coexistence of  $N1$  minimum with other minima. To get these results, we have done multiple scans over the parameter space. In each of these scans, the percentages are computed after generating a large number of parametric points (at least 15000), which satisfy the bounds of Eqs. (43) and (44).

In Table III, we have given numerical results on coexistence of the  $N1$  and  $N3$  minima. In order to search for this coexistence, in our scan over parameters of the scalar potential, we satisfy the minimization conditions only for  $N1$  and  $N3$ . As a result of this, from Table II, we notice that the relations for  $\mu_1^2$  and  $\mu_2^2$  are fixed, but  $\mu_3^2$  can be chosen arbitrarily. Moreover, the quantity  $v_{\eta(3)}$  can also be chosen arbitrarily. In our scan, we have varied  $v_{\eta(3)}$  and  $\mu_3^2$  randomly in the ranges of  $(-100, 100)$  GeV and  $(-10^5, 10^5)$  GeV<sup>2</sup>, respectively. For these ranges of  $v_{\eta(3)}$  and  $\mu_3^2$ , we have found that the percentages given in Table III to be large. In Table III, we have chosen  $A$ -parameter to be suppressed as compared to the electroweak scale since this parameter should be small, which is described previously. From this table, we see that there is nearly a 44% chance in finding the  $N1$  minimum. On the other hand, there is around a 15% chance in finding a parametric point for which both  $N1$  and  $N3$  are minima. From the last column of Table III, we see that around 11% of the points correspond to the  $N1$  minimum to be deeper than the  $N3$  minimum, in terms of potential depth. In this table, the difference of percentages between the second and third columns, for a particular value of  $A$ , is about 29%. This percentage corresponds to the parametric region in which  $N1$  is the only minimum. We see here that, out of the total area of scan, in a significant fraction of it,  $N1$  is the only minimum. From this table, we see that the numerical results are not sensitive to the  $A$ -parameter. Moreover, by changing the sign of  $A$ , we nearly got the same percentages that are given in Table III.

After satisfying only the minimization conditions for  $N1$  and  $N4$  in our scanning procedure, we have obtained numerical results on the coexistence of these minima. These results are given in Table IV. In a region where  $N1$  and  $N4$  coexist, the parameters  $\mu_{2,3}^2$  are fixed according

TABLE III. For various values of  $A$ , percentages of coexistence between the minima  $N1$  and  $N3$  are given. In the second column, percentage of existence of  $N1$  minimum is given. In the third column, percentage of coexistence of  $N1$  and  $N3$  is given. In the fourth column, percentage of coexistence of  $N1$  and  $N3$  with  $V_{N1} < V_{N3}$  is given.

$\frac{A}{v_{EW}}$	$N1$	$N1$ and $N3$	$N1$ deeper than $N3$
0.1	43.3%	15.2%	11.1%
$10^{-3}$	43.6%	14.7%	10.6%
$10^{-5}$	43.7%	15.1%	11.0%

TABLE IV. Percentages of coexistence between the minima  $N1$  and  $N4$  are given. The columns in this table are analogous to that in Table III.

$\frac{A}{v_{EW}}$	$N1$	$N1$ and $N4$	$N1$ deeper than $N4$
0	33.5%	18.3%	12.3%

to the relations given in Table II. Here, the quantities  $v_{\eta(4)}$  and  $v_{\chi(4)}$  can be chosen arbitrarily. We have varied these quantities independently in the range  $(-100, 100)$  GeV in order to obtain percentages in Table IV. For this particular range of values, the percentages given in this table are large. We notice that the minima  $N1$  and  $N4$  coexist in a region where  $A = 0$ . For this value of  $A$ , and from the discussion given below Eq. (4), the neutrino masses in this model become zero. Hence, in order to explain nonzero masses to neutrinos, we should choose  $A \neq 0$ , and thereby, the coexistence between  $N1$  and  $N4$  can be avoided.

In analogy to the results described for Tables III and IV, we have searched for the coexistence of the minima  $N1$  and  $N5$ . The results of this coexistence are given in Table V. In order to get results in this table, we have varied  $v_{\chi(5)}$  and  $\mu_2^2$  in the ranges  $(-100, 100)$  GeV and  $(-10^5, 10^5)$  GeV<sup>2</sup>, respectively. From this table, we see that the percentages are not sensitive to the value of  $A$ . Moreover, we have seen that these results are not sensitive to the sign of  $A$ . After comparing the results in Tables III and V, we see that the percentage of coexistence between  $N1$  and  $N5$  is lower as compared to that between  $N1$  and  $N3$ .

In Table VI, we have given the results on the coexistence of the minima  $N1$  and  $N8$ . These results are obtained after

TABLE V. Percentages of coexistence between the minima  $N1$  and  $N5$  are given. The columns in this table are analogous to that in Table III.

$\frac{A}{v_{EW}}$	$N1$	$N1$ and $N5$	$N1$ deeper than $N5$
0.1	36.0%	9.4%	7.8%
$10^{-3}$	36.0%	9.5%	8.1%
$10^{-5}$	36.4%	9.3%	8.0%

TABLE VI. Percentages of coexistence between the minima  $N1$  and  $N8$  are given. The columns in this table are analogous to that in Table III.

$\frac{ A }{v_{EW}}$	$N1$	$N1$ and $N8$	$N1$ deeper than $N8$
0.1	26.4%	4.8%	4.2%
$10^{-3}$	21.0%	0.57%	0.56%
$10^{-5}$	21.4%	0.14%	0.14%
0	21.7%	0%	0%

satisfying only the minimization conditions of  $N1$  and  $N8$ . Among these conditions, the relation for  $\mu_1^2$  gives a constraint relation. This relation is satisfied by solving for unknown  $\lambda$  parameters, and later we have checked if these  $\lambda$  parameters obey the conditions of Eqs. (43) and (44). While obtaining the results in Table VI, we have varied each of  $v_{\phi(8)}, v_{\eta(8)}, v_{\chi(8)}$  independently in the range  $(-100, 100)$  GeV, for which the percentages in this table are found to be large. After comparing the results in this table with that of Tables III and V, we see that the percentage of coexistence for  $N1$  and  $N8$  is lower than that for  $N1$  with either  $N3$  or  $N5$ . In Table VI, we have given the value of  $|A|$  since the sign of  $A$  is determined by the sign of  $v_{\phi(8)}v_{\eta(8)}v_{\chi(8)}$  in our scanning procedure. This is due to the fact that we have a condition of Eq. (22) for the minimum  $N8$ . We notice that by decreasing the value of  $|A|$ , the percentage for coexistence between the minima  $N1$  and  $N8$  is getting decreased. We have found that, for  $A = 0$ , the minimum  $N8$  exists in some region of parameter space. However,  $N8$  minimum does not coexist with  $N1$  minimum in the region where  $A = 0$ . In the numerical analysis, we have noticed that  $N8$  becomes a saddle point in the region where  $N1$  is a minimum, for  $A = 0$ .

In our scanning procedure, we have searched for the coexistence of minima  $N1$  and  $C11$ . While satisfying the minimization conditions of these minima, the relation for  $\mu_1^2$  gives a constraint relation. This is solved in an analogous way of what we have described for Table VI. We have varied the quantities  $v_{\phi(11)}, c_{\eta(11)}, v_{\eta(11)}, v_{\chi(11)}$  arbitrarily in our analysis. Now, we see that the parameter  $A$  is determined by the above quantities through one of the minimization conditions of  $C11$ , which is given in Table II. As already described before, the parameter  $A$  should be small in order to be consistent with the model framework. As a result of this, we have demanded  $\frac{|A|}{v_{EW}} \leq 0.1$  in our analysis, and thereafter, we have not found a region for the coexistence of the minima  $N1$  and  $C11$ . In the Appendix, we argue that for  $A$  to be a negligibly small variable,  $C11$  becomes a saddle point in the region where  $N1$  is a minimum. The result shown in this appendix, concurs with our numerical result that the minima  $N1$  and  $C11$  do not coexist for  $A$  to be a small variable. On the other hand, in our analysis, for  $\frac{|A|}{v_{EW}} > 0.1$ , we have found a region for the coexistence of minima  $N1$  and  $C11$ . However, this region is not viable due to the above mentioned reasons.

In the previous section we have argued that, even if the minimum  $N1$  coexists with either of the minima  $N2, N6, N7, C9$ , or  $C10$ , the potential depth at  $N1$  is always deeper than that at the other minima mentioned here. For the sake of completeness, in our numerical analysis, we have searched if  $N1$  coexists with any of the above mentioned minima. This search is done in an analogous way of what we have described for the results of Tables III–VI. In our analysis, we have not found a region where  $N1$  coexists

with either of the minima  $N2, N6, N7, C9$ , or  $C10$ . In the Appendix, we argue that some of these SPs become saddle points in a region where  $N1$  is a minimum.

From the numerical results presented so far, we have seen that in the Dirac scotogenic model, the minimum  $N1$  can coexist with either of the minima  $N3, N4, N5$ , or  $N8$ . Here, it should be noted that the coexistence of the minima  $N1$  and  $N4$  happen in a region where  $A = 0$ . This region is not interesting since neutrino masses become zero in this region of the model. On the other hand, the coexistence of  $N1$  with the other minima of  $N3, N5$ , and  $N8$  can happen in a region where  $A \neq 0$ , which is an interesting region to us from the point of neutrino masses. Hence, in this region, we have searched to see if the  $N1$  minimum coexists with more than one minima of  $N3, N5$  and  $N8$ . In Table VII, we have given results on the coexistence of the minima among  $N1, N3$ , and  $N5$ . While obtaining results on this coexistence, we have satisfied minimization conditions only for these minima. Also, for these results, we have varied  $v_{\eta(3)}$  and  $v_{\chi(5)}$  independently in the range  $(-100, 100)$  GeV. We see that the percentage of coexistence among these minima is far less than that given in Tables III and V. We have noticed that the percentages given in Table VII are not sensitive to the value of  $A$ , which is also the case in Tables III and V.

We have also searched for the coexistence of minima among  $N1, N3$ , and  $N8$  and also among  $N1, N5$ , and  $N8$ . In our analysis, we have found that the above mentioned coexistences can happen in a region of  $\frac{|A|}{v_{EW}} > 0.1$ . However, this region is not viable since  $A$  should be a small parameter. Hence, we have demanded  $\frac{|A|}{v_{EW}} \leq 0.1$  in our analysis, and thereafter, we have not found a region for the above mentioned coexistences. This result may be understood in the following way. In Table VI, it is shown that in the limit that  $A$  is small, the percentage of chances for  $N8$  to coexist with  $N1$  is getting decreased. Hence, for small  $A$ , it is difficult for  $N8$  to coexist with  $N1$  and  $N3$  or with  $N1$  and  $N5$ . Finally, we have found that the minima  $N1, N3, N5$ , and  $N8$  can coexist in a region of  $\frac{|A|}{v_{EW}} > 0.1$ , but otherwise, we have not found a region for these minima to coexist.

While describing the results of Table III, we have mentioned that the difference in the percentages of the second and third columns corresponds to the fraction of the total scanned region, where  $N1$  is the only minimum. This statement is true even for Tables IV–VII. In any of these tables, the difference in the percentages of the second and third columns, for a particular value of  $A$ , is at least 15%.

TABLE VII. Percentages of coexistence among the minima  $N1, N3$ , and  $N5$  are given. The columns in this table are analogous to that in Table III.

$\frac{A}{v_{EW}}$	$N1$	$N1, N3$ and $N5$	$N1$ deeper than $N3, N5$
0.1	32.9%	0.81%	0.77%

After comparing percentages in these tables, we notice that in a significant parameter region of our scanning process,  $N1$  is the only minimum. Moreover, in this region,  $N1$  is obviously the global minimum of the Dirac scotogenic model. On the other hand, there exist a certain parameter region where  $N1$  can coexist with other minima, whose percentage of chances of finding is given by the third column of Tables III–VII. In the region where  $N1$  coexists with other minima, we have demanded that the potential depth at  $N1$  is lower than that at the other minima, so that  $N1$  can be the global minimum of this model. The fourth column of Tables III–VII gives the percentage of chances for  $N1$  to be the global minimum in the region where it coexists with other minima.

## VI. HIGGS TO DIPHOTON DECAY

In the previous section, we have described the status of the  $N1$  minimum as the global minimum of the Dirac scotogenic model. We have noticed that the analysis of the previous section is determined by the parameters of the scalar potential. We now want to study the impact of this analysis on phenomenological observable quantities. One of the observable quantities is the decay  $H \rightarrow \gamma\gamma$  upon which the scalar sector of this model can have an impact. This decay is, in general, driven by charged particles through a loop induced process. In the Dirac scotogenic model, this decay gets additional contribution due to the  $\eta^+$  field. This decay is the subject of experimental investigation since it can distinguish any new physics signals from that of the SM. As part of this investigation, in the LHC experiment, the signal strength of  $H \rightarrow \gamma\gamma$  is measured, and it is found to be  $1.1 \pm 0.07$  [8]. In this section, we compute the signal strength of this decay in the Dirac scotogenic model and study consequences on this quantity due to analysis of the previous section.

The signal strength of  $H \rightarrow \gamma\gamma$  is defined as the ratio of the observed cross section of  $pp \rightarrow H \rightarrow \gamma\gamma$  against to the same quantity computed in the SM. The observed cross section of  $pp \rightarrow H \rightarrow \gamma\gamma$  in the LHC experiment should match with that computed in the model of our work, which is the Dirac scotogenic model. We notice that the production cross section for the Higgs boson in the Dirac scotogenic model is nearly the same as that in the SM since the dominant process for this production is through the gluon fusion. As a result of this, after using the narrow width approximation, the signal strength of  $H \rightarrow \gamma\gamma$  in our work is given by

$$R_{\gamma\gamma} = \frac{\text{Br}(H \rightarrow \gamma\gamma)_{\text{DSM}}}{\text{Br}(H \rightarrow \gamma\gamma)_{\text{SM}}} = \frac{\Gamma(H \rightarrow \gamma\gamma)_{\text{DSM}}}{\Gamma(H \rightarrow \gamma\gamma)_{\text{SM}}} \frac{\Gamma_{\text{SM}}^H}{\Gamma_{\text{DSM}}^H}. \quad (46)$$

Here, the quantities having the suffixes DSM and SM are the ones computed in the Dirac scotogenic and standard models, respectively.  $\Gamma_{\text{DSM,SM}}^H$  correspond to the total decay widths of the Higgs boson in the above two models. The decay widths of  $H \rightarrow \gamma\gamma$ , which are required in Eq. (46), are computed using a general expression for this quantity given in [39]. For the case of the Dirac scotogenic model, we have

$$\begin{aligned} \Gamma(H \rightarrow \gamma\gamma)_{\text{DSM}} &= \frac{\alpha^2 G_F m_H^3}{128 \sqrt{2} \pi^3} \left| \sum_f N_f Q_f^2 F_{1/2}(\beta_f) + F_1(\beta_W) \right. \\ &\quad \left. + \frac{\lambda_3 v_{\text{EW}}^2}{m_{\eta^+}^2} F_0(\beta_\eta) \right|^2, \\ \beta_f &= \frac{4m_f^2}{m_H^2}, \quad \beta_W = \frac{4m_W^2}{m_H^2}, \quad \beta_\eta = \frac{4m_{\eta^+}^2}{m_H^2}, \end{aligned} \quad (47)$$

where  $\alpha$  and  $G_F$  are fine-structure and Fermi constants, respectively. Here,  $N_f$ ,  $Q_f$  and  $m_f$  are color factor, charge, and mass of SM fermion, respectively. After excluding the last term in the modulus of the above equation, we get the expression for  $\Gamma(H \rightarrow \gamma\gamma)_{\text{SM}}$ . The  $F$ -functions in Eq. (47) are the form factors of spin-1/2, -1, and -0 fields, which drive the decay  $H \rightarrow \gamma\gamma$ . These functions are given below:

$$\begin{aligned} F_{1/2}(\beta) &= -2\beta[1 + (1 - \beta)f(\beta)], \\ F_1(\beta) &= 2 + 3\beta + 3\beta(2 - \beta)f(\beta), \\ F_0(\beta) &= \beta[1 - \beta f(\beta)], \\ f(\beta) &= \begin{cases} \left(\sin^{-1} \frac{1}{\sqrt{\beta}}\right)^2, & \beta \geq 1. \\ -\frac{1}{4} \left[ \ln \frac{1 + \sqrt{1 - \beta}}{1 - \sqrt{1 - \beta}} - i\pi \right]^2, & \beta < 1 \end{cases} \end{aligned} \quad (48)$$

While computing  $R_{\gamma\gamma}$  in our analysis, we have taken the total decay width of Higgs boson in the SM as  $\Gamma_{\text{SM}}^H = 4.1 \times 10^{-3}$  GeV [40]. Now, the total decay width of Higgs boson in the Dirac scotogenic model, to a leading order, is given by

$$\begin{aligned} \Gamma_{\text{DSM}}^H &= \Gamma_{\text{SM}}^H + \Gamma(H \rightarrow \zeta_1 \zeta_1) + \Gamma(H \rightarrow \zeta_1 \zeta_2) \\ &\quad + \Gamma(H \rightarrow \zeta_2 \zeta_2) + \Gamma(H \rightarrow \zeta_3 \zeta_3) \\ &\quad + \Gamma(H \rightarrow \eta^+ \eta^-). \end{aligned} \quad (49)$$

In the above equation, the partial decay widths of Higgs boson into scalar particles of the Dirac scotogenic model are computed using tree level couplings of these processes. These couplings are given below:

$$\begin{aligned} C_{H\zeta_1\zeta_1} &= -i\sqrt{2}v_{\text{EW}}[(\lambda_3 + \lambda_4 + \lambda_5)O_{12}^2 + \lambda_7 O_{22}^2] \\ &\quad - i2A O_{12} O_{22}, \\ C_{H\zeta_1\zeta_2} &= -i\sqrt{2}v_{\text{EW}}[(\lambda_3 + \lambda_4 + \lambda_5)O_{11} O_{12} + \lambda_7 O_{21} O_{22}] \\ &\quad - iA(O_{12} O_{21} + O_{11} O_{22}), \\ C_{H\zeta_2\zeta_2} &= -i\sqrt{2}v_{\text{EW}}[(\lambda_3 + \lambda_4 + \lambda_5)O_{11}^2 + \lambda_7 O_{21}^2] \\ &\quad - i2A O_{11} O_{21}, \\ C_{H\zeta_3\zeta_3} &= -i\sqrt{2}(\lambda_3 + \lambda_4 - \lambda_5)v_{\text{EW}}, \\ C_{H\eta^+\eta^-} &= -i\sqrt{2}\lambda_3 v_{\text{EW}}. \end{aligned} \quad (50)$$

Here,  $O_{ij}$ , where  $i, j = 1, 2$ , is the element of an orthogonal matrix which diagonalizes the mixing mass matrix of  $\eta_R^0$  and  $\chi$ , which is given in Eq. (3). In our numerical analysis, we follow the below convention for the diagonalization of this mixing matrix,

$$O^T M_{\eta_R^0 \chi}^2 O = \text{diag}(m_{\zeta_2}, m_{\zeta_1}). \quad (51)$$

Here we identify  $m_{\zeta_1}$  to be the lightest.

Using the expressions which are described above, we have computed  $R_{\gamma\gamma}$  after scanning over parameters of the scalar potential of the Dirac scotogenic model. We notice here that while scanning over these parameters, it is possible that the  $N1$  minimum of this model may coexist with other minima of the model. In order to see the effect of this coexistence, we have done the scanning in a way of what we have described in the previous section. The difference in the scanning of the previous section and the current section is that, in the current analysis, we have taken  $m_{\zeta_1}$  as the lightest among the masses of additional particles of the Dirac scotogenic model. It is to remind here that the additional particles of this model are charged under  $Z_2^{(B)}$  symmetry, which is exact. Hence,  $\zeta_1$  is a possible candidate for the dark matter. As a result of this, we have applied the following constraints in the current analysis:

$$m_{\eta^+} > 105 \text{ GeV}, \quad 5 \text{ GeV} < m_{\zeta_1} < m_{\zeta_{2,3}}, m_{\eta^+}. \quad (52)$$

The results of our analysis, after doing a generic scan over parameters, are given in Fig. 1.

We see that many points exist in the left-hand side plot as compared to that in the right-hand side plot of Fig. 1. This implies that many parametric points in our scan correspond to the points where  $N1$  is the only minimum. This result is also described in the numerical analysis of the previous

section. From the plots of Fig. 1, we see that for  $m_{\zeta_1} < m_H/2$ ,  $R_{\gamma\gamma}$  is suppressed. This suppression is due to the factor  $\frac{\Gamma_{\text{DSM}}^H}{\Gamma^H}$  in  $R_{\gamma\gamma}$ . For  $m_{\zeta_1} < m_H/2$ , the decay channel  $H \rightarrow \zeta_1 \zeta_1$  opens up, whose decay width is found to be at least about 0.1 GeV, which gives the necessary suppression in the above mentioned factor. Also, in Fig. 1, we have found that the points, for which  $m_{\zeta_1} < m_H/2$ , do not satisfy the constraint due to invisible decay of Higgs boson. For  $m_{\zeta_1} < m_H/2$ , the Higgs boson of this model decays invisibly, whose branching ratio is constrained to be  $Br_{H \rightarrow \text{inv}} < 0.145$  [41]. In order to get enhancement of  $R_{\gamma\gamma}$  for  $m_{\zeta_1} < m_H/2$ , one has to suppress the couplings of Higgs to scalar particles, whose expressions are given in Eq. (50). In the scanning process, after including the above mentioned constraint on  $Br_{H \rightarrow \text{inv}}$ , we have seen that the suppression in couplings is possible, and thereby,  $R_{\gamma\gamma}$  can be enhanced to within the experimentally allowed region, for  $m_{\zeta_1} < m_H/2$ . On the other hand, for  $m_{\zeta_1} > m_H/2$ , there will not be suppression in  $\frac{\Gamma_{\text{DSM}}^H}{\Gamma^H}$ . Hence, a majority of the points are within the experimentally allowed region, for  $m_{\zeta_1} > m_H/2$ .

In both the plots of Fig. 1, for  $m_{\zeta_1} > m_H/2$ , the points are around the horizontal line, which corresponds to the lower  $3\sigma$  allowed value of  $R_{\gamma\gamma}$ . Moreover, we see that only a few points give the enhancement of  $R_{\gamma\gamma} > 1$ . In this regard, see Refs. [42–47] where enhancement of  $R_{\gamma\gamma} > 1$  has been reported in various models. Below we describe the reasons for not getting much enhancement in  $R_{\gamma\gamma}$  in the plots of Fig. 1. As already explained before, for  $m_{\zeta_1} > m_H/2$ , we get  $\frac{\Gamma_{\text{DSM}}^H}{\Gamma^H} = 1$ . Hence, in the region of  $m_{\zeta_1} > m_H/2$ , we get  $R_{\gamma\gamma} > 1$  only if  $\lambda_3 < 0$  since  $\beta_\eta > 1$ . The value of  $\lambda_3$  is constrained by the bounded from below conditions of Eq. (44). After satisfying these conditions, we have noticed

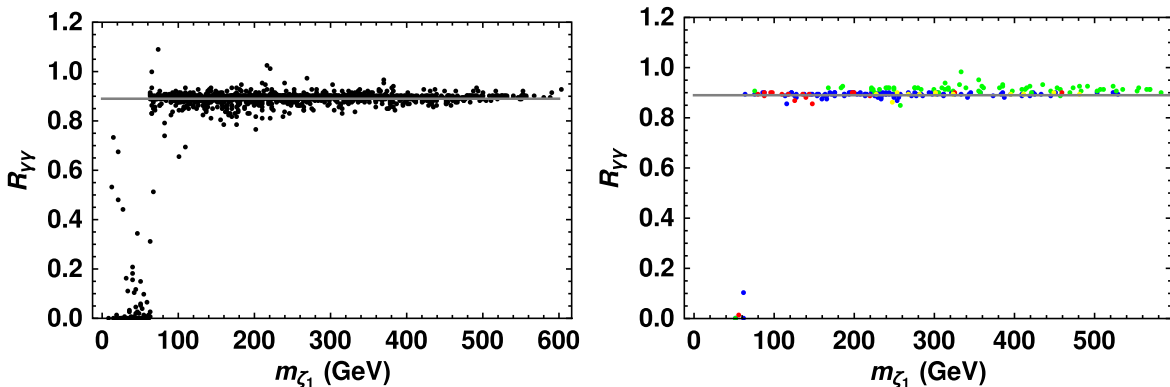


FIG. 1. The left-hand side plot is for parametric points for which  $N1$  is the only minimum. Right-hand side plot is for parametric points where the  $N1$  minimum coexists with other minima of the model, and moreover, for these points, the potential depth at  $N1$  is deeper than that at other minima. In the right-hand side plot, blue, green, red, and yellow are the points where  $N1$  minimum coexists with  $N3$ ,  $N5$ ,  $N8$ , and  $N3 + N5$  minima, respectively. The horizontal line in these plots indicates the experimentally allowed lower  $3\sigma$  value of  $R_{\gamma\gamma}$ . In these plots, we have taken  $\frac{|A|}{v_{\text{EW}}} = 0.01$ .

that  $\lambda_3 > -2$ . Since the negative values of  $\lambda_3$  are restricted by these conditions, we do not get much enhancement in  $R_{\gamma\gamma}$  in our work. On the other hand, in our scanning procedure, we have seen that by restricting  $m_{\eta^+}$  to as low as 130 GeV, it is possible for  $R_{\gamma\gamma}$  to be as high as 1.3.

In the region where  $N1$  minimum coexists with  $N3$  minimum, we do not get  $R_{\gamma\gamma} > 1$ . This is due to the fact that, in this region, we have  $\mu_2^2 < 0$  because of the minimization condition of  $N3$ . As a result of this, in order to get  $m_{\eta^+}^2 > 0$  we should have  $\lambda_3 > 0$ , and thereby we get  $R_{\gamma\gamma} < 1$ . Similarly, in the region where  $N1$  and  $N8$  minima coexist, we have found  $\lambda_3 > 0$  in the scanning analysis, and hence, we get  $R_{\gamma\gamma} < 1$ . On the other hand, in the region where  $N1$  and  $N5$  minima coexist,  $\mu_2^2$  is a free parameter. Hence, in this region, we can choose  $\mu_2^2 > 0$ , and thereby  $\lambda_3$  can be negative, so that  $R_{\gamma\gamma} > 1$ . Now, it should be clear that in a region where  $N1$  is the only minimum, we can get  $\mu_2^2 > 0$ , and thereby, we get  $R_{\gamma\gamma} > 1$ . From the above described results, we see that the future determination of  $R_{\gamma\gamma}$  by the LHC experiment can have an impact on the study of global minimum of this model. It is to be noted that a precise determination of  $R_{\gamma\gamma}$  in the LHC experiment can distinguish the above described vacuum realizations. On the other hand, if the error bar is large enough so that the allowed value of  $R_{\gamma\gamma}$  is around 1, then the above vacuum realizations may not be distinguished. Finally, from Fig. 1, we notice that the experimentally allowed values of  $R_{\gamma\gamma}$  can be fitted in the Dirac scotogenic model, irrespective of the fact that the  $N1$  minimum either coexists or not with other minima of this model.

## VII. POSSIBILITY OF A SCALAR DARK MATTER

It is described in Sec. II that, due to exact symmetry of  $Z_2^{(B)}$ , the lightest among the additional particles of the Dirac scotogenic model is a candidate for dark matter. We notice that the lightest among the singlet Dirac fermions  $N_k^D$  is a possible candidate for dark matter. In the original model [21], this possibility has been studied, and it is shown that  $N_1^D$  can consistently explain the dark matter phenomenology. See Ref. [48], for another work in this direction. In the present work, since our motivation is to study the scalar sector of the Dirac scotogenic model, we study on the possibility of scalar dark matter in this model.

In the previous section, it is described that, while obtaining the results of Fig. 1, we have taken  $\zeta_1$  as the lightest particle among the additional particles of the Dirac scotogenic model. From Eq. (3), we notice that  $\zeta_1$  is an admixture of  $\eta_R^0$  and  $\chi$ . For sufficiently small  $A$ , which is the case in Fig. 1,  $\eta_R^0$  and  $\chi$  are nearly equal to the mass eigenstates of this model. In such a case,  $\zeta_1$  is dominantly made of either  $\eta_R^0$  or  $\chi$ , depending on the parameter choice

of the model. We see that the scalar dark matter in this model is either part of an  $SU(2)_L$  doublet or a singlet field. We first consider the case of  $\zeta_1$  being dominantly made of  $\chi$  and analyze if this case can consistently explain all the dark matter phenomenology. Later we analyze the case where  $\zeta_1$  is dominantly made of  $\eta_R^0$ .

In the phenomenology of dark matter, we need to explain the relic abundance of dark matter in the present Universe and also the null results of direct and indirect searches for dark matter detection. The current relic density of dark matter is  $0.12 \pm 0.0012$  [49]. In order to explain this relic density, we need to compute thermally averaged pair-annihilation cross section of dark matter times the relative velocity of these particles, which is denoted by  $\langle\sigma v_{\text{rel}}\rangle$ . To a good approximation, for a cold dark matter, the above mentioned relic density can be fitted if  $\langle\sigma v_{\text{rel}}\rangle \approx 3 \times 10^{-26} \text{ cm}^3/\text{s} = 1 \text{ pb}$  [8]. In the Dirac scotogenic model, for the case of dark matter  $\zeta_1 \approx \chi$ , the possible pair-annihilation processes at tree level are as follows:

$$\zeta_1 \zeta_1 \rightarrow \nu_i^D \bar{\nu}_j^D, \quad (53)$$

$$\zeta_1 \zeta_1 \rightarrow HH, \quad (54)$$

$$\zeta_1 \zeta_1 \rightarrow H^* \rightarrow f\bar{f}, W^+W^-, ZZ, HH. \quad (55)$$

Here,  $H^*$  is virtual Higgs boson, and  $f$  is any SM fermion.  $\nu_i^D$  are the mass eigenstates of the neutrino fields of the Dirac scotogenic model.

The reaction in Eq. (53) is driven by the  $h_{k\alpha}$  couplings of Eq. (1), via a  $t$ -channel process mediated by the singlet fermions  $N_k^D$ . We can take the mass of  $N_k^D$  ( $m_{N_k}$ ) to be around 1 TeV and the couplings  $h_{k\alpha} \sim 1$ . For these values of  $m_{N_k}$  and  $h_{k\alpha}$ , and from the discussion given below Eq. (4), we see that it is possible to explain small masses to neutrinos either by suppressing the  $A$ -parameter or by taking degenerate masses to  $\zeta_{1,2}$ . Now the annihilation cross section for the process in Eq. (53) is given by

$$\begin{aligned} \sigma(\zeta_1 \zeta_1 \rightarrow \nu_i^D \bar{\nu}_j^D) v_{\text{rel}} \\ = \frac{1}{8\pi} \sum_k \frac{|\sum_{\alpha,\beta} h_{k\alpha} V_{\alpha i}^* h_{k\beta}^* V_{\beta j}|^2}{(m_{\zeta_1}^2 + m_{N_k}^2)^2} (m_{\nu_i}^2 + m_{\nu_j}^2). \end{aligned} \quad (56)$$

Here,  $V_{\alpha i}$  are the elements of  $V$ , which diagonalize the neutrino mass matrix, which is discussed in Sec. II. For neutrino masses around 0.1 eV, the above pair-annihilation cross section is suppressed by 14 orders of magnitude as compared to the required amount. Hence, the process in Eq. (53) cannot explain the relic density of dark matter.

The processes in Eqs. (54) and (55) are driven due to quartic and trilinear couplings of  $\zeta_1$  to the Higgs field, and these couplings are proportional to  $\lambda_7$ , for  $\zeta_1 \approx \chi$ . By taking  $m_{\zeta_1} = 200 \text{ GeV}$  and  $\lambda_7 = 0.1$ , we have found the

following pair-annihilation cross sections for the processes of Eqs. (54) and (55):

$$\begin{aligned} \sigma_{v_{\text{rel}}|\bar{t}t} &= 0.17 \text{ pb}, & \sigma_{v_{\text{rel}}|WW} &= 0.94 \text{ pb}, \\ \sigma_{v_{\text{rel}}|ZZ} &= 0.44 \text{ pb}, & \sigma_{v_{\text{rel}}|HH} &= 0.51 \text{ pb}. \end{aligned} \quad (57)$$

We see that the cross section into  $WW$  channel is dominant among all possible pair-annihilations of  $\zeta_1$ . The above cross section values decrease with increasing  $m_{\zeta_1}$ . From these cross section values, we see that, for few hundred GeV of mass to  $\zeta_1$  and for  $\lambda_7 \sim 0.1$ , using the processes of Eqs. (54) and (55), the relic abundance of dark matter can be fitted in this model. However, in this model, the trilinear coupling of  $\zeta_1$  to the Higgs field also drives the process of dark matter scattering against a nucleus. This process has been searched in many dark matter experiments [50–52], which use xenon as the target nucleus. Since no sign of dark matter is found in these experiments, upper bounds on the cross section of dark matter against a nucleon have been obtained. In the Dirac scotogenic model, using [53], we estimate the spin-independent cross section of  $\zeta_1 \approx \chi$  with xenon nucleus as

$$\begin{aligned} \sigma_0 &= \frac{1}{\pi} \left( \frac{m_{\zeta_1} m_{Xe}}{m_{\zeta_1} + m_{Xe}} \right)^2 \left| \frac{54f_p + 77f_n}{131} \right|^2, \\ \frac{f_p}{m_p} &= \left[ 0.075 + \frac{2}{27}(1 - 0.075) \right] \frac{\lambda_7}{m_{\zeta_1} m_H^2}, \\ \frac{f_n}{m_n} &= \left[ 0.078 + \frac{2}{27}(1 - 0.078) \right] \frac{\lambda_7}{m_{\zeta_1} m_H^2}. \end{aligned} \quad (58)$$

Here,  $m_p$ ,  $m_n$ , and  $m_{Xe}$  are masses of proton, neutron, and xenon nucleus, respectively. As stated before, upper bounds on  $\sigma_0$  have been set due to null results of dark matter detection in various experiments. Among these, the most stringent limit is  $\sigma_0 < 6.5 \times 10^{-48} \text{ cm}^2$  [52]. In order to satisfy this limit, in the Dirac scotogenic model, we get  $\lambda_7 < 4.8 \times 10^{-5}$  for  $m_{\zeta_1} \sim 100 \text{ GeV}$ . For this suppressed value of  $\lambda_7$  and for no fine tuning in the mass of  $m_{\zeta_1}$ , we see that the cross sections in the processes of Eqs. (54) and (55) are highly suppressed, and we cannot fit the relic abundance of dark matter in this model. On the other hand, for a fine tuned mass of  $m_{\zeta_1} \approx m_H/2$ , via the process  $\zeta_1 \zeta_1 \rightarrow H^* \rightarrow b\bar{b}$ , the relic abundance of dark matter can be fitted for  $\lambda_7 = 1.3 \times 10^{-5}$ , which also satisfies the upper limit on  $\sigma_0$ . However, from the indirect searches of dark matter, the thermal annihilation cross section of dark matter into the  $b\bar{b}$  channel has been ruled out for dark matter mass of up to 300 GeV [54]. As a result of this, we see that the processes in Eqs. (54) and (55) cannot consistently explain the dark matter phenomenology, for the case of  $\zeta_1 \approx \chi$ .

Now, we consider the case  $\zeta_1 \approx \eta_R^0$ , where the dark matter is dominantly made up of a component of  $SU(2)_L$  doublet. In this case, in order to explain the relic density of dark matter, pair-annihilation of  $\zeta_1$  through the processes

given in Eqs. (53)–(55) can be analyzed. It should be noted that the process of Eq. (53) happens for the case  $\zeta_1 \approx \eta_R^0$  through the  $f_{ak}$  couplings of Eq. (1). As a result of this, pair-annihilation cross section for this process is analogous to that of Eq. (56), where  $h_{ka} V_{ai}^*$  should be replaced by  $f_{ak}^* U_{ai}^*$ . Now, we see that, due to small masses to neutrinos, this pair-annihilation cross section is highly suppressed as compared to the required amount in order to explain the relic density of dark matter. The processes in Eqs. (54) and (55) are driven by the quartic and trilinear couplings of  $\zeta_1$  to the Higgs field. We see that, for the case  $\zeta_1 \approx \eta_R^0$ , these couplings are proportional to  $\lambda_3 + \lambda_4 + \lambda_5$ . As a result of this, the cross section values of Eq. (57) are also applicable to the case  $\zeta_1 \approx \eta_R^0$ , where we take  $m_{\zeta_1} = 200 \text{ GeV}$  and  $\lambda_3 + \lambda_4 + \lambda_5 = 0.1$ . Hence, the relic density of dark matter can be fitted for the case  $\zeta_1 \approx \eta_R^0$ . However, analogous to what we described above, due to nonobservation of dark matter in direct detection experiments, the quantity  $\lambda_3 + \lambda_4 + \lambda_5$  should be suppressed to around  $10^{-5}$ . As a result of this, the processes in Eqs. (54) and (55) cannot consistently explain the relic density of dark matter, for the case  $\zeta_1 \approx \eta_R^0$ . Apart from the processes of Eqs. (53)–(55), due to gauge interactions, the following annihilations are also possible for the case of  $\zeta_1 \approx \eta_R^0$ ,

$$\zeta_1 \zeta_1 \rightarrow W^+ W^-, \quad \zeta_1 \zeta_1 \rightarrow ZZ, \quad \zeta_1 \zeta_1 \rightarrow W^+ W^- \gamma \gamma. \quad (59)$$

In the above equation, the first two annihilations happen due to quartic interactions and the third annihilation happens due to mediation of  $\eta^+$  field at tree level. Moreover, for  $m_{\zeta_1} < m_{W,Z}$ , one of the  $V = W^\pm, Z$  in the first two processes of Eq. (59) can be off shell, and thereby, we get 3- and 4-body final states from the annihilation products of  $VV^*$  and  $V^*V^*$ , respectively. *A priori*, for  $m_{\zeta_1} \gtrsim m_W$ , the first process of Eq. (59) can give the required amount of thermal annihilation cross section in order to fit the relic density of dark matter. Moreover, constraints due to indirect detection of dark matter from pair-annihilation into gauge bosons are weaker [54]. Nevertheless, the first two processes of Eq. (59) can induce scattering between  $\zeta_1$  and a nucleus at 1-loop level. In fact, there exist other 1-loop processes, which are mediated by gauge interactions, for the above mentioned scattering. Although this scattering happens at 1-loop level, given the strong constraints on this due to direct detection experiments, we may expect it is challenge for  $\zeta_1 \approx \eta_R^0$  to evade these constraints.

## VIII. COMPARISON WITH THE SCOTOGENIC MODEL

In this section, we compare the phenomenology of the Dirac scotogenic model with that of the scotogenic model [16], where neutrinos are Majorana particles. It is described in Sec. II that there is an analogy between these

two models in terms of field content and also from the viewpoint of neutrino masses and mixing. Here, we describe some more analogies between these two models in terms of phenomenological observable quantities of dark matter, LFV, and collider signals.

In the previous section, we have discussed the status of scalar dark matter in the Dirac scotogenic model. We have discussed two possibilities, where in one case  $\zeta_1 \approx \chi$  and in the other case  $\zeta_1 \approx \eta_R^0$ . Now, below we compare the scalar dark matter phenomenology of this model with that of the scotogenic model [16]. It is to remind here that in the scotogenic model, the singlet field  $\chi$  does not exist. Hence, a possibility for scalar dark matter in the scotogenic model is  $\zeta_1 = \eta_R^0$ . As a result of this, the phenomenological discussion we have given in the previous section for the case of  $\zeta_1 \approx \eta_R^0$  is applicable to the scotogenic model. A difference in the scotogenic model is that, in addition to the process of Eq. (53), the following process  $\zeta_1 \zeta_1 \rightarrow \nu_i^M \nu_j^M$  can also happen, which violates the lepton number. Here,  $\nu_i^M$  is a neutrino field of the scotogenic model, which is a Majorana particle. The above process is mediated in the scotogenic model by the analogous couplings of  $f_{ak}$ , which are given in Eq. (1). As already described below Eq. (1), in the scotogenic model, there exist  $N_k^M$  field, instead of  $(N_k, N_k^c)$ . The field  $N_k^M$  is Majorana in the scotogenic model. As a result of this, the annihilation cross section for the above process is found to be

$$\sigma(\zeta_1 \zeta_1 \rightarrow \nu_i^M \nu_j^M) v_{\text{rel}} = \frac{S}{16\pi} \sum_k \left| \sum_{\alpha, \beta} f_{ak} U_{ai} f_{\beta k} U_{\beta j} \right|^2 \times \frac{M_k^2}{(M_k^2 + m_{\zeta_1}^2)^2}. \quad (60)$$

Here,  $M_k$  is the mass of  $N_k^M$  field of the scotogenic model, and  $S$  is a symmetry factor which is 1(2) for  $i \neq j$  ( $i = j$ ). For  $f_{ak} \sim 1$ ,  $m_{\zeta_1} \sim 100$  GeV and  $M_k = 2.78$  TeV, the above pair-annihilation cross section is around 1 pb, which is the required amount in order to fit the relic abundance of dark matter. Moreover, it looks like there exist no constraints on the above pair-annihilation cross section from experiments. On the other hand, see Refs. [55–57] for indirect searches of dark matter, where an upper limit on the pair-annihilation cross section of dark matter into  $\nu\bar{\nu}$  mode is set to around  $10^{-24}$  cm<sup>3</sup>/s. As a result of the above description, in the scotogenic model, it is possible to fit the relic density of dark matter and avoid the indirect detection bounds on it. However, as already described in the previous section, the first two processes of Eq. (59) can induce scattering of  $\zeta_1$  with a nucleus at 1-loop level. The loop diagrams for this scattering are driven by gauge couplings and are mediated by SM fields. Hence, it appears that the amplitude of these diagrams have only the loop suppression factor. It may be worth it to compute the cross section for

the above scattering in order to see if it satisfies the direct detection bound [52] on the dark matter.

As described in Sec. II, there is a region of parameter space where the couplings  $f_{ak}$  can be of order 1 and these couplings drive LFV processes [8] in the Dirac scotogenic model. So far none of the LFV processes are observed in experiments, and upper bounds have been set on the branching ratios of various LFV decays and also on the conversion rate of  $\mu$  to  $e$  in a nucleus [8]. Among the LFV decays, stringent limits exist on the branching ratios of  $\mu \rightarrow e\gamma$  [58] and  $\mu \rightarrow 3e$  [59]. The above mentioned LFV processes are driven in the Dirac scotogenic model due to mediation of  $\eta^+$  and  $N_k^D$  at 1-loop level. Analyzing LFV processes is out of the scope of this paper. Nevertheless, in our work, experimental limits on these processes can be satisfied by taking the masses of  $\eta^+$  or  $N_k^D$  to be sufficiently high, for  $f_{ak} \sim 1$ . In addition to this, there is also a possibility of suppressing the couplings  $f_{ak}$  in order to satisfy the above experimental limits.

Below, we compare the Dirac scotogenic and scotogenic models in terms of LFV processes. As stated before, Feynman diagrams for LFV processes in the Dirac scotogenic model are driven by  $\eta^+$  and  $N_k^D$ . Whereas, in the scotogenic model [16], the corresponding Feynman diagrams are driven by  $\eta^+$  and  $N_k^M$ , where  $N_k^M$  is an additional Majorana field. In the scotogenic model, LFV processes have been analyzed in [60]. We see that, in the Feynman diagrams for LFV processes of scotogenic model, one should replace the  $N_k^M$ -propagator with  $N_k^D$ -propagator in order to get the corresponding Feynman diagrams of the Dirac scotogenic model. As a result of this, by interchanging the mass of  $N_k^M$  with  $N_k^D$ , we get the same branching ratio expressions for  $\mu \rightarrow e\gamma$  in both these models. However, the branching ratio expression for  $\mu \rightarrow 3e$  should be different in these models, which is explained below. The amplitude for  $\mu \rightarrow 3e$  arises from the following contributions in both these models:  $\gamma$ -penguin, Z-penguin, Higgs-penguin and box diagrams. The penguin diagrams should give the same kind of expressions for amplitude in both these models, due to the above mentioned replacement of propagators. On the other hand, the box diagrams of the scotogenic model involve diagrams which are due to the Dirac and Majorana nature of the  $N_k^M$ -propagator. Whereas, these diagrams are driven only due to the Dirac nature of the  $N_k^D$ -propagator in the Dirac scotogenic model. As a result of this, we get additional contribution to box diagrams in the scotogenic model as compared to that of the Dirac scotogenic model. Now, we see that the expression for the conversion rate of  $\mu$  to  $e$  should be the same in both these models since this conversion happens due to penguin diagrams.

The additional fields in the Dirac scotogenic model are  $N_k^D$ ,  $\eta^+$  and  $\zeta_i$ ,  $i = 1, 2, 3$ . The best way to test this model in collider experiments is by probing the  $\eta^+$  field. Note that  $\eta^+$  can be produced in the LHC experiment via gauge

interactions, and it decays as  $\eta^+ \rightarrow \ell^+ N_1^D$  or  $\eta^+ \rightarrow W^+ \zeta_1$ . Here,  $N_1^D$  is the lightest among  $N_k^D$ . The above two decays give us missing energy plus a charged lepton or a dijet signal, depending on the decay channel of  $W$ . Analyzing collider signals of this model is out of the scope of this work. However, see Refs. [61,62] for some collider analysis on scalar sector in related models. The above described signal in the Dirac scotogenic model is also possible in the scotogenic model. The difference between these two models in terms of field content is the presence of the singlet scalar field  $\chi$  in the Dirac scotogenic model. Since the singlet field does not experience gauge interactions, it is a challenge to probe the existence of  $\chi$  field in the Dirac scotogenic model. Hence, one needs to develop some techniques to distinguish the above two models in collider experiments. It is worth it to do a detailed analysis on this aspect in the future.

## IX. CONCLUSIONS

In this work, we have studied on the vacuum structure of the scalar potential of the Dirac scotogenic model. One of the motivations of this model is to explain neutrino masses through a radiative mechanism and also to have Dirac nature to the neutrinos. The other motivation is to have a stable dark matter candidate. After analyzing the scalar potential of this model, we have found that 11 different minima are possible. Out of these 11, the  $N1$  minimum of Eq. (6) is the desired minimum of this model. Only with this minimum, the motivations of this model can be achieved consistently. As a result of this, we have worked to see if the  $N1$  minimum can be made as the global minimum of this model. Through our numerical analysis, we have shown that plenty of parameter space exists where  $N1$  is the global minimum. In our numerical analysis, we have found that the  $N1$  minimum can coexist with certain other minima in some regions of parameter space. However, in the viable parameter space of this model, we have not found the coexistence of the  $N1$  minimum with charge-breaking minima. We have justified this statement with an analytical demonstration to it in the Appendix.

We have studied the Higgs to diphoton decay in this model since the scalar sector of this model has an implication on this decay. After doing a generic scan over parameters of the scalar potential, we have found that the signal strength of this decay can be within the experimentally allowed region, but most likely to be around the lower  $3\sigma$  allowed value of this quantity. With some tuning of the parameters, the signal strength of this decay is found to be as high as 1.3. In the numerical analysis, we have found that the experimentally allowed values of this quantity can be explained irrespective of the fact that the  $N1$  minimum coexists with other minima or not.

Finally, we have studied the possibility of making the lightest among the additional scalar particles of this model, as a candidate for dark matter. We have found that the

singlet scalar field of this model cannot be a viable candidate for dark matter. This we have found, due to the fact that the current bounds from the direct and indirect detection of dark matter in experiments rule out the possibility of explaining the relic density of dark matter. The other possibility for scalar dark matter in this model is the  $\eta_R^0$  field, which is a component of the  $SU(2)_L$  doublet. In this case, we have found that constraints due to direct detection bounds on the dark matter are difficult to be satisfied.

## APPENDIX: SADDLE POINTS

From the numerical analysis of Sec. V, we have noticed that certain minima do not coexist with the  $N1$  minimum. Below we present analytical calculations through which we justify why some of these minima do not coexist with the  $N1$  minimum. Our methodology in these calculations is based on the discussions given in [12,38].

In Sec. V, it is described that, by demanding  $\frac{|A|}{v_{EW}} \leq 0.1$  in our numerical analysis, we have not found a region of coexistence between the minima  $C11$  and  $N1$ . Here we show that, in the limit that  $A$  is a negligibly small parameter,  $C11$  becomes a saddle point in the region where  $N1$  is a minimum. From the minimization conditions of  $C11$ , which are given in Table II, we notice that  $A$  becomes a small variable if either  $\lambda_4 + \lambda_5$  or  $v_{\phi(11)} v_{\eta(11)} / v_{\chi(11)}$  is suppressed. As a result of this, we neglect terms involving the above mentioned variables in comparison to other terms of the scalar potential. Now, apart from satisfying the minimization conditions of  $C11$ , we need to evaluate the mass-square eigenvalues of the scalar fields in order to check if  $C11$  becomes a minimum or not. For calculating these eigenvalues, we have described the parametrization of scalar fields of a SP in Eq. (23). We express these scalar fields in the following basis:  $\varphi = (\phi_R^1, \phi_I^1, \eta_R^1, \eta_I^1, \phi_R^0, \phi_I^0, \eta_R^0, \eta_I^0, \chi_R)$ . Now, the general form of the mixing mass-square matrix among the scalar fields of a SP is given by

$$[M^2]_{ij} = \frac{\partial^2 V}{\partial \varphi_i \partial \varphi_j} = \frac{\partial^2 V}{\partial x_l \partial x_m} \frac{\partial x_l}{\partial \varphi_i} \frac{\partial x_m}{\partial \varphi_j} + \frac{\partial V}{\partial x_l} \frac{\partial^2 x_l}{\partial \varphi_i \partial \varphi_j}. \quad (\text{A1})$$

Here,  $i, j = 1, \dots, 9$  and  $x_l$ , where  $l = 1, \dots, 5$ , are defined in Eq. (24).

The last term of Eq. (A1) becomes zero for the case of  $C11$  since after using the minimization conditions we get  $\frac{\partial V}{\partial x_l} = 0$ . As a result of this, for the SP  $C11$ , Eq. (A1) becomes  $M_{C11}^2 = Y^T B Y$ . Here,  $Y$  and  $B$  are matrices of orders  $5 \times 9$  and  $5 \times 5$ , respectively. The elements of these matrices are given below:

$$[Y]_{li} = \frac{\partial x_l}{\partial \varphi_i}, \quad [B]_{lm} = \frac{\partial^2 V}{\partial x_l \partial x_m} = [M_4]_{lm} + \frac{\partial^2 V_3}{\partial x_l \partial x_m}. \quad (\text{A2})$$

In the limit that  $A$  is a small variable, the matrix  $B$  takes the following form:

$$B = \begin{pmatrix} & 0 & 0 \\ B_1 & 0 & 0 \\ & \frac{A}{v_{\chi(11)}} & 0 \\ 0 & 0 & \frac{A}{v_{\chi(11)}} & 2(\lambda_4 + \lambda_5) & 0 \\ 0 & 0 & 0 & 0 & 2(\lambda_4 - \lambda_5) \end{pmatrix},$$

$$B_1 = \begin{pmatrix} \lambda_1 & \lambda_3 & \frac{1}{2}\lambda_7 \\ \lambda_3 & \lambda_2 & \frac{1}{2}\lambda_8 \\ \frac{1}{2}\lambda_7 & \frac{1}{2}\lambda_8 & \frac{1}{2}\lambda_6 \end{pmatrix}. \quad (\text{A3})$$

Now, as it is argued in [12], it is possible to express the matrix  $M_{C11}^2$  in the following block form:

$$M_{C11}^2 = \begin{pmatrix} 0 & 0 \\ 0 & Y'^r B Y' \end{pmatrix}. \quad (\text{A4})$$

Here,  $Y'$  is a  $5 \times 5$  matrix which depends only on the VEVs of  $C11$ . From the above form of  $M_{C11}^2$ , we see that  $C11$  has four Goldstone bosons. This is expected since the SP  $C11$  breaks the electroweak and charge symmetries, which are continuous. Also, from the above equation, we see that, if all the eigenvalues of  $B$  are positive (negative), then  $M_{C11}^2$  is positive (negative) definite, and thus,  $C11$  is minimum (maximum). On the other hand, if  $B$  has both positive and negative eigenvalues, then  $C11$  becomes a saddle point. Now, in the limit that  $A$  is a small variable, the first three eigenvalues of  $B$  are determined by that of  $B_1$ . We see that  $\text{Tr}(B_1) > 0$ , due to the conditions of Eq. (44). As a result of this,  $B$  has at least one positive eigenvalue, in the limit that  $A$  is a small variable.

In Eq. (42), we have given the difference in potential depths at the stationary points  $C11$  and  $N1$ . In the limit that  $A$  is a small variable, the last term of Eq. (42) can be neglected. Moreover, in this limiting process,  $m_3^2 + \lambda_7 v_{EW}^2$  is nearly equal to one of the eigenvalues of the scalar fields of the SP  $N1$ . Hence, in a region where  $N1$  is a minimum and in the above limiting process, we get  $V_{C11} - V_{N1} > 0$ . To get the expression for  $V_{C11} - V_{N1}$ , we have used the general expression of Eq. (32). Here, we see that  $X_{N1}^T V'_{C11} = 0$ . Hence, in the limit that  $A$  is a small variable, we get  $V_{C11} - V_{N1} \approx \frac{1}{2} X_{C11}^T V'_{N1}$ . Now, we define  $\tilde{X}_{C11}$ ,  $\tilde{X}_{N1}$ ,  $\tilde{V}'_{N1}$ , and  $\tilde{M}_2$  as 3-column matrices, whose elements are the first three elements of  $X_{C11}$ ,  $X_{N1}$ ,  $V'_{N1}$ , and  $M_2$ , respectively. With these definitions and in the above limiting process, we get the following relation:

$$\left. \frac{\partial V}{\partial x_i} \right|_{C11} = 0 \Rightarrow \tilde{X}_{C11} \approx -B_1^{-1} \tilde{M}_2. \quad (\text{A5})$$

After using the above relation, we get

$$\begin{aligned} V_{C11} - V_{N1} &\approx \frac{1}{2} X_{C11}^T V'_{N1} = \frac{1}{2} \tilde{X}_{C11}^T \tilde{V}'_{N1} \\ &= -\frac{1}{2} \tilde{V}'_{N1} B_1^{-1} \tilde{M}_2 = -\frac{1}{2} \tilde{V}'_{N1} B_1^{-1} (\tilde{V}'_{N1} - B_1 \tilde{X}_{N1}) \\ &= -\frac{1}{2} \tilde{V}'_{N1} B_1^{-1} \tilde{V}'_{N1}. \end{aligned} \quad (\text{A6})$$

Earlier we have argued that  $V_{C11} - V_{N1} > 0$  in a region where  $N1$  is a minimum. Hence, after using the above relation, we see that  $B_1$  should not be a positive definite matrix, and thus, one of the eigenvalues of  $B_1$  is negative. As a result of this, in the limit that  $A$  is a small variable, one of the eigenvalues of  $B$  is negative. Combining this result with the earlier result that  $B$  has at least one positive eigenvalue, we see that  $C11$  becomes a saddle point in a region where  $N1$  is a minimum and also that  $A$  is a negligibly small variable.

The above described result on the nature of  $C11$  is valid even if  $A = 0$ . However, for  $A = 0$ , we get  $\lambda_4 + \lambda_5 = 0$ , and thus, the inverse of  $B$  does not exist. To circumvent this problem, we have used  $B_1$ , which is a submatrix of  $B$ , in the above described analysis.

The above described analysis can be applied to other SPs of  $N2$ ,  $C9$ , and  $C10$ , in order to show that these become saddle points in the region where  $N1$  is a minimum. The difference we encounter is that the last term of Eq. (A1) does not vanish for the above mentioned SPs. As a result of this, we have explicitly computed the mixing masses for the scalar fields of the above SPs. For instance, in the case of  $C9$ , we have found that the fields  $\eta_R^1$ ,  $\phi_R^0$ , and  $\eta_R^0$  mix together, whose masses are given by

$$Z^T \tilde{B} Z, \quad \tilde{B} = \begin{pmatrix} \lambda_2 & \lambda_3 & \lambda_2 \\ \lambda_3 & \lambda_1 & \lambda_3 \\ \lambda_2 & \lambda_3 & \lambda_2 \end{pmatrix},$$

$$Z = \begin{pmatrix} c_{\eta(9)} & 0 & 0 \\ 0 & v_{\phi(9)} & 0 \\ 0 & 0 & v_{\eta(9)} \end{pmatrix}. \quad (\text{A7})$$

Now, using an analogous formalism described for the case of  $C11$ , we can show that the matrix  $\tilde{B}$  has one positive and one negative eigenvalue, apart from a zero eigenvalue. As a result of this,  $C9$  becomes a saddle point in a region where  $N1$  is a minimum.

In Sec. V, we have mentioned that the minima  $N6$  and  $N7$  do not coexist with the  $N1$  minimum. Moreover, we have also described that the percentage of coexistence between the minima  $N8$  and  $N1$  is zero for  $A = 0$ . All the above mentioned SPs become saddle points in a region where  $N1$  is a minimum. We have realized this statement through our numerical analysis, but otherwise, we do not have an analytical proof for this.

- [1] ATLAS Collaboration, Observation of a new particle in the search for the standard model Higgs boson with the ATLAS detector at the LHC, *Phys. Lett. B* **716**, 1 (2012).
- [2] CMS Collaboration, Observation of a new boson at a mass of 125 GeV with the CMS experiment at the LHC, *Phys. Lett. B* **716**, 30 (2012).
- [3] P. W. Higgs, Broken symmetries, massless particles and gauge fields, *Phys. Lett.* **12**, 132 (1964).
- [4] P. W. Higgs, Broken Symmetries and the Masses of Gauge Bosons, *Phys. Rev. Lett.* **13**, 508 (1964).
- [5] P. W. Higgs, Spontaneous symmetry breakdown without massless bosons, *Phys. Rev.* **145**, 1156 (1966).
- [6] F. Englert and R. Brout, Broken Symmetry and the Mass of Gauge Vector Mesons, *Phys. Rev. Lett.* **13**, 321 (1964).
- [7] G. S. Guralnik, C. R. Hagen, and T. W. B. Kibble, Global Conservation Laws and Massless Particles, *Phys. Rev. Lett.* **13**, 585 (1964).
- [8] Particle Data Group, Review of particle physics, *Prog. Theor. Exp. Phys.* **2022**, 083C01 (2022).
- [9] C. Quigg, Beyond the standard model in many directions, in *Proceedings of the 2nd CERN-CLAF School of High Energy Physics* (2004), pp. 57–118, [arXiv:hep-ph/0404228](https://arxiv.org/abs/hep-ph/0404228).
- [10] J. Ellis, Physics beyond the standard model, *Nucl. Phys.* **A827**, 187C (2009).
- [11] T. D. Lee, A theory of spontaneous  $T$  violation, *Phys. Rev. D* **8**, 1226 (1973).
- [12] P. M. Ferreira, R. Santos, and A. Barroso, Stability of the tree-level vacuum in two Higgs doublet models against charge or  $CP$  spontaneous violation, *Phys. Lett. B* **603**, 219 (2004).
- [13] A. Barroso, P. M. Ferreira, and R. Santos, Charge and  $CP$  symmetry breaking in two Higgs doublet models, *Phys. Lett. B* **632**, 684 (2006).
- [14] I. P. Ivanov, Minkowski space structure of the Higgs potential in 2HDM, *Phys. Rev. D* **75**, 035001 (2007).
- [15] I. P. Ivanov, Minkowski space structure of the Higgs potential in 2HDM. II. Minima, symmetries, and topology, *Phys. Rev. D* **77**, 015017 (2008).
- [16] E. Ma, Verifiable radiative seesaw mechanism of neutrino mass and dark matter, *Phys. Rev. D* **73**, 077301 (2006).
- [17] I. F. Ginzburg, K. A. Kanishev, M. Krawczyk, and D. Sokolowska, Evolution of Universe to the present inert phase, *Phys. Rev. D* **82**, 123533 (2010).
- [18] P. M. Ferreira and B. Swiezewska, One-loop contributions to neutral minima in the inert doublet model, *J. High Energy Phys.* **04** (2016) 099.
- [19] G. Cacciapaglia and M. Rosenlyst, Loop-generated neutrino masses in composite Higgs models, *J. High Energy Phys.* **09** (2021) 167.
- [20] M. Rosenlyst, Technically natural Higgs boson from Planck scale, *Phys. Rev. D* **106**, 013002 (2022).
- [21] Y. Farzan and E. Ma, Dirac neutrino mass generation from dark matter, *Phys. Rev. D* **86**, 033007 (2012).
- [22] E. Ma and O. Popov, Pathways to naturally small Dirac neutrino masses, *Phys. Lett. B* **764**, 142 (2017).
- [23] W. Wang, R. Wang, Z.-L. Han, and J.-Z. Han, The  $B - L$  scotogenic models for Dirac neutrino masses, *Eur. Phys. J. C* **77**, 889 (2017).
- [24] E. Ma, Scotogenic  $U(1)_X$  Dirac neutrinos, *Phys. Lett. B* **793**, 411 (2019).
- [25] J. Leite, A. Morales, J. W. F. Valle, and C. A. Vaquera-Araujo, Scotogenic dark matter and Dirac neutrinos from unbroken gauged  $B - L$  symmetry, *Phys. Lett. B* **807**, 135537 (2020).
- [26] S.-Y. Guo and Z.-L. Han, Observable signatures of scotogenic Dirac model, *J. High Energy Phys.* **12** (2020) 062.
- [27] N. Bernal, J. Calle, and D. Restrepo, Anomaly-free Abelian gauge symmetries with Dirac scotogenic models, *Phys. Rev. D* **103**, 095032 (2021).
- [28] D. Borah, E. Ma, and D. Nanda, Dark  $SU(2)$  gauge symmetry and scotogenic Dirac neutrinos, *Phys. Lett. B* **835**, 137539 (2022).
- [29] J. A. Casas and A. Ibarra, Oscillating neutrinos and  $\mu \rightarrow e, \gamma$ , *Nucl. Phys.* **B618**, 171 (2001).
- [30] R. S. Hundi, Lepton flavor violating  $Z$  and Higgs decays in the scotogenic model, *Eur. Phys. J. C* **82**, 505 (2022).
- [31] G. C. Branco, P. M. Ferreira, L. Lavoura, M. N. Rebelo, M. Sher, and J. P. Silva, Theory and phenomenology of two-Higgs-doublet models, *Phys. Rep.* **516**, 1 (2012).
- [32] P. M. Ferreira and B. L. Gonçalves, Stability of neutral minima against charge breaking in the Higgs triplet model, *J. High Energy Phys.* **02** (2020) 182.
- [33] J. Velhinho, R. Santos, and A. Barroso, Tree level vacuum stability in two Higgs doublet models, *Phys. Lett. B* **322**, 213 (1994).
- [34] C. C. Nishi,  $CP$  violation conditions in  $N$ -Higgs-doublet potentials, *Phys. Rev. D* **74**, 036003 (2006).
- [35] M. Maniatis, A. von Manteuffel, O. Nachtmann, and F. Nagel, Stability and symmetry breaking in the general two-Higgs-doublet model, *Eur. Phys. J. C* **48**, 805 (2006).
- [36] I. P. Ivanov and C. C. Nishi, Symmetry breaking patterns in 3HDM, *J. High Energy Phys.* **01** (2015) 021.
- [37] P. M. Ferreira, The vacuum structure of the Higgs complex singlet-doublet model, *Phys. Rev. D* **94**, 096011 (2016).
- [38] P. M. Ferreira, M. Mühlleitner, R. Santos, G. Weiglein, and J. Wittbrodt, Vacuum instabilities in the N2HDM, *J. High Energy Phys.* **09** (2019) 006.
- [39] M. A. Shifman, A. I. Vainshtein, M. B. Voloshin, and V. I. Zakharov, Low-energy theorems for Higgs boson couplings to photons, *Sov. J. Nucl. Phys.* **30**, 711 (1979).
- [40] LHC Higgs Cross Section Working Group, Handbook of LHC Higgs cross sections: 3. Higgs properties, [arXiv:1307.1347](https://arxiv.org/abs/1307.1347).
- [41] ATLAS Collaboration, Search for invisible Higgs-boson decays in events with vector-boson fusion signatures using  $139 \text{ fb}^{-1}$  of proton-proton data recorded by the ATLAS experiment, *J. High Energy Phys.* **08** (2022) 104.
- [42] A. Arhrib, R. Benbrik, and N. Gaur,  $H \rightarrow \gamma\gamma$  in inert Higgs doublet model, *Phys. Rev. D* **85**, 095021 (2012).
- [43] B. Swiezewska and M. Krawczyk, Diphoton rate in the inert doublet model with a 125 GeV Higgs boson, *Phys. Rev. D* **88**, 035019 (2013).
- [44] A. G. Akeroyd and S. Moretti, Enhancement of  $H \rightarrow \gamma\gamma$  from doubly charged scalars in the Higgs triplet model, *Phys. Rev. D* **86**, 035015 (2012).
- [45] R. S. Hundi, Implications of Higgs boson to diphoton decay rate in the bilinear  $R$ -parity violating supersymmetric model, *Phys. Rev. D* **87**, 115005 (2013).
- [46] C.-X. Yue, Q.-Y. Shi, and T. Hua, Vector bileptons and the decays  $h \rightarrow \gamma\gamma, Z\gamma$ , *Nucl. Phys.* **B876**, 747 (2013).

- [47] I. García-Jiménez, J. Montaña, G. I. Nápoles-Cañedo, H. Novales-Sánchez, J. J. Toscano, and E. S. Tututi, Diphoton Higgs signal strength in universal extra dimensions, *J. Phys. G* **47**, 105003 (2020).
- [48] D. K. Ghosh, S. Jeusun, and D. Nanda, Long-lived inert Higgs boson in a fast expanding universe and its imprint on the cosmic microwave background, *Phys. Rev. D* **106**, 115001 (2022).
- [49] Planck Collaboration, Planck 2018 results. VI. Cosmological parameters, *Astron. Astrophys.* **641**, A6 (2020).
- [50] XENON Collaboration, Dark Matter Search Results from a One Ton-Year Exposure of XENON1T, *Phys. Rev. Lett.* **121**, 111302 (2018).
- [51] PandaX-4T Collaboration, Dark Matter Search Results from the PandaX-4T Commissioning Run, *Phys. Rev. Lett.* **127**, 261802 (2021).
- [52] LZ Collaboration, First dark matter search results from the LUX-ZEPLIN (LZ) experiment, [arXiv:2207.03764](https://arxiv.org/abs/2207.03764).
- [53] E. Ma, Non-Abelian gauge lepton symmetry as the gateway to dark matter, *Phys. Lett. B* **819**, 136456 (2021).
- [54] K. N. Abazajian, S. Horiuchi, M. Kaplinghat, R. E. Keeley, and O. Macias, Strong constraints on thermal relic dark matter from Fermi-LAT observations of the Galactic Center, *Phys. Rev. D* **102**, 043012 (2020).
- [55] Super-Kamiokande Collaboration, Indirect search for dark matter from the Galactic Center and halo with the Super-Kamiokande detector, *Phys. Rev. D* **102**, 072002 (2020).
- [56] ANTARES Collaboration, Search for dark matter towards the Galactic Centre with 11 years of ANTARES data, *Phys. Lett. B* **805**, 135439 (2020).
- [57] IceCube Collaboration, Search for neutrinos from dark matter self-annihilations in the center of the Milky Way with 3 years of IceCube/DeepCore, *Eur. Phys. J. C* **77**, 627 (2017).
- [58] MEG Collaboration, Search for the lepton flavour violating decay  $\mu^+ \rightarrow e^+\gamma$  with the full dataset of the MEG experiment, *Eur. Phys. J. C* **76**, 434 (2016).
- [59] SINDRUM Collaboration, Search for the decay  $\mu^+ \rightarrow e^+e^+e^-$ , *Nucl. Phys.* **B299**, 1 (1988).
- [60] T. Toma and A. Vicente, Lepton flavor violation in the scotogenic model, *J. High Energy Phys.* **01** (2014) 160.
- [61] S. von Buddenbrock, N. Chakrabarty, A. S. Cornell, D. Kar, M. Kumar, T. Mandal, Bruce Mellado, Biswarup Mukhopadhyaya, Robert G. Reed, and Xifeng Ruan, Phenomenological signatures of additional scalar bosons at the LHC, *Eur. Phys. J. C* **76**, 580 (2016).
- [62] A. Crivellin, Y. Fang, O. Fischer, A. Kumar, M. Kumar, E. Malwa *et al.*, Accumulating evidence for the associate production of a neutral scalar with mass around 151 GeV, [arXiv:2109.02650](https://arxiv.org/abs/2109.02650).